

**PURDUE UNIVERSITY
GRADUATE SCHOOL
Thesis/Dissertation Acceptance**

This is to certify that the thesis/dissertation prepared

By Liuying Du

Entitled

CHARACTERIZING THE IMPACT OF CLIMATE AND LAND USE CHANGE ON BLUE AND GREEN WATER OVER THE OHIO RIVER BASIN, U.S.

For the degree of Master of Science in Civil Engineering

Is approved by the final examining committee:

VENKATESH M. MERWADE

Chair

DENNIS A. LYN

INDRAJEET CHAUBEY

To the best of my knowledge and as understood by the student in the Thesis/Dissertation Agreement, Publication Delay, and Certification Disclaimer (Graduate School Form 32), this thesis/dissertation adheres to the provisions of Purdue University's "Policy of Integrity in Research" and the use of copyright material.

Approved by Major Professor(s): VENKATESH M. MERWADE

Approved by: DULCY M. ABRAHAM

Head of the Departmental Graduate Program

4/12/2016

Date

CHARACTERIZING THE IMPACT OF CLIMATE AND LAND USE CHANGE ON
BLUE AND GREEN WATER OVER THE OHIO RIVER BASIN, U.S.

A Thesis

Submitted to the Faculty

of

Purdue University

by

Liuying Du

In Partial Fulfillment of the

Requirements for the Degree

of

Master of Science in Civil Engineering

May 2016

Purdue University

West Lafayette, Indiana

For my beloved parents and boyfriend

ACKNOWLEDGEMENTS

I would like to thank my advisor Prof. Venkatesh Merwade for his constant support, time and guidance. I appreciate his hours of work spent meticulously to improve the quality of my writing and research. I would also like to thank Prof. Dennis Lyn and Prof. Indrajeet Chaubey for serving on my committee.

I would also like to thank my colleague Adnan Rajib for his support and guidance throughout my research. I also would like to thank Kuk Hyun Ahn for providing land use data. This research cannot be accomplished without their assistance.

I would like to thank the helping hands and support from my colleagues in the hydraulics and hydrology group. They have given me great help both academically and spiritually during the past two years.

.

TABLE OF CONTENTS

	Page
LIST OF TABLES	vii
LIST OF FIGURES	viii
LIST OF ABBREVIATIONS.....	x
ABSTRACT.....	xii
CHAPTER 1. INTRODUCTION.....	1
1.1 Background	1
1.2 Literature Review.....	2
1.3 Research Objectives	4
1.4 Thesis Organization	5
CHAPTER 2. STUDY AREA AND DATA INPUT	6
2.1 Introduction	6
2.2 Study Area	7
2.3 Input Data	9
CHAPTER 3. METHODOLOGY.....	13
3.1 Introduction	13

	Page
3.2 Model Description.....	13
3.3 Model Setup	14
3.4 Tile Drainage	16
3.5 Model Calibration, Parameterization, and Validation	17
3.5.1 Calibration Method	17
3.5.2 Calibration Procedure.....	19
3.6 Trend Analysis	22
3.6.1 Mann-Kendall Test.....	22
3.6.2 Theil-Sen Test	29
3.7 Separation of Climate and Land Use Change Impacts.....	29
CHAPTER 4. RESULTS	32
4.1 Introduction	32
4.2 Land Use and Climate Change.....	32
4.2.1 Land Use Change	32
4.2.2 Climate Change	35
4.2.3 Regional Characterization	38

	Page
4.3 Model Evaluation	41
4.4 Trend Analysis in Sub-basin Scale	44
4.5 Trend analysis in Basin and Regional Scale	48
4.6 Relative Contributions of Climate and Land Use Change	52
CHAPTER 5. DISCUSSION	56
5.1 Climate Impacts on BW	56
5.2 Climate Impacts on GW.....	57
5.3 Land Use Impact on BW	58
5.4 Land use impact on GW.....	59
5.5 Uncertainty Analysis	59
5.6 Limitations	61
5.7 Future Forecast	63
CHAPTER 6. SUMMARY AND CONCLUSION.....	64
LIST OF REFERENCES.....	67

LIST OF TABLES

Table	Page
Table 2.1 Calibration and Validation Sites Information.....	12
Table 3.1 KGE for Uncalibrated Models.....	20
Table 3.2 SWAT Calibration Parameters	21
Table 4.1 Climate Change Based on TS Result with 95% Confidence Interval.....	35
Table 4.2 Regional Comparison of Climate and Land Use Change in ORB.....	41
Table 4.3 Goodness-of-Fit Scores for Calibration and Validation Sites	42
Table 4.4 Comparison of KGE between Uncalibrated and Calibrated Models.....	43
Table 4.5 Best Estimates of Calibrated Parameters	43
Table 4.6 Volumetric Magnitudes of BW and GW Changes	51
Table 4.7 Relative Contributions to BW and GW	54
Table 4.8 Relative Contributions to Each Water Component of BW and GW	55

LIST OF FIGURES

Figure	Page
Figure 2.1 Study Area and Weather Station Location	7
Figure 2.2 Calibration and Validation Station Location.....	11
Figure 3.1 Autocorrelation for Annual Precipitation.....	24
Figure 3.2 Autocorrelation for Annual Minimum Temperature.....	25
Figure 3.3 Autocorrelation for Annual Maximum Temperature	26
Figure 3.4 Autocorrelation for BW.....	27
Figure 3.5 Autocorrelation for GW	28
Figure 4.1 Percentage of Land Use from Historical and SWAT Maps	33
Figure 4.2 Land Use Maps from 1940s to 2010s.....	34
Figure 4.3 MK Test for the Average Annual Precipitation (mm yr ⁻¹)	36
Figure 4.4 MK Test for Annual Maximum, Mean, and Minimum Temperature	37
Figure 4.5 Annual Precipitation Change in Sub-basin Scale.....	38

Figure	Page
Figure 4.6 Regional Division Based on Climate and Land Use Change	40
Figure 4.7 MK Test for GW in the Sub-basin Scale	45
Figure 4.8 MK Test for BW in the Sub-basin Scale	46
Figure 4.9 MK Test with TS Slope for BW and GW in the Basin Scale	48
Figure 4.10 MK Test with TS Slope for BW and GW in the Regional Scale	50
Figure 4.11 Volumetric Magnitudes of BW and GW with Confidence Interval.....	52

LIST OF ABBREVIATIONS

BW	Blue Water
DEM	Digital Elevation Model
ET	Evapotranspiration
GW	Green Water
HEMA	Human-Environmental Modeling and Analysis
MK	Mann-Kendall Statistics method
NCDC	National Climate Data Center
NLCD	National Land Cover Dataset
ORB	Ohio River Basin
PET	Potential Evapotranspiration
STATSGO	State Soil Geographic Data
SUFI-2	Sequential Uncertainty Fitting Version 2

SWAT	Soil and Water Assessment Tool
TS	Theil-Sen approach
USGS	United States Geological Survey
WCB	Western Corn Belt

ABSTRACT

Liuying Du. M.S.C.E., Purdue University, May 2016. Characterizing the Impact of Climate and Land Use Change on Blue and Green Water over the Ohio River Basin, U.S. Major Professor: Venkatesh Merwade.

Impacts of climate and land use change on the overall water availability can be quantified in terms of long-term trends in surface and subsurface hydrologic fluxes. This study presents the spatio-temporal characterization of Blue Water (BW) and Green Water (GW) dynamics during the period of 1935 to 2014 in the Ohio River Basin (ORB). The combined and relative contributions of climate and land use changes to BW and GW dynamics are also quantified. The Soil and Water Assessment Tool (SWAT) is used to simulate hydrologic components, and trend analyses (Mann-Kendall and Theil-Sen tests) are performed on the model outputs to detect the trend and magnitude of trends in BW and GW at three different levels, namely the entire basin, regional, and sub-basin levels. Precipitation increase and land use change from agriculture to forest are detected as the dominant indicators of climate and land use change in ORB. As a result, BW and GW in the entire basin has increased due to the combined effects of climate and land use change, but sub-basin and regional results reveal a distinctive spatial pattern. GW has increased

significantly in the upper and lower parts of the basin, which can be related to the prominent land use change in those areas; while BW has increased significantly only in the lower part, likely being associated with the notable precipitation change there. Climate change influences BW significantly, but relatively nominally on GW, whereas land use change increases GW remarkably, but has an opposing effect on BW. These results help to understand the collective influence of natural and anthropogenic impacts on hydrologic responses in the ORB, and thereby provide useful information for future water security and planning.

CHAPTER 1. INTRODUCTION

1.1 Background

Climate and land use changes such as global warming, extreme weather events, and urbanization are occurring at an unprecedented rate (Asselen & Verburg, 2013; Goldewijk, 2001; Meehl et al., 2007; Stocker et al., 2014), and have great impacts on global and regional hydrologic fluxes (Allen et al., 1998; Eshleman, 2004). This kind of hydrologic change challenges conventional water resources planning and management. In order to have a better understanding of hydrologic changes, many researchers have tried to quantify the individual or combined effects of climate and land use change on water resources (Gupta et al., 2015; Mishra et al., 2010; van Roosmalen et al., 2009). These studies have reported significant hydrologic changes due to climate or land use change.

Current studies are primarily focused on conventional blue water (BW) stored in rivers, lakes, reservoirs, or aquifers, which is estimated to contain nearly one third of the total available fresh water (Falkenmark & Rockström, 2006). The remaining two-thirds of the total fresh water, known as green water (GW), is stored in soils and plants and circulates within the water cycle through evapotranspiration (ET) feedbacks (Falkenmark, 1995). By definition, BW is the sum of surface runoff and deep aquifer recharge; GW is the sum

of actual ET and soil moisture. BW is critical for domestic and industrial water consumption, whereas GW plays a key role in vegetation growth, and consequently in crop production (Falkenmark & Rockström, 2006; Rockström et al., 2009). Quantitative assessment of BW helps to manage domestic and industrial water supply and provide information for the probabilities of extreme events such as floods and droughts; understanding the change of GW helps to improve agricultural productivity and solve the world hunger problem. Therefore, it is necessary to identify the spatio-temporal pattern of BW and GW and correlate them to climate and land use change.

1.2 Literature Review

Several studies have assessed BW and GW availability by using large scale models. For example, Schuol et al. (2008), Faramarzi et al. (2009), and Abbaspour et al. (2015) modelled the availability and spatial distribution of BW and GW in Western Africa, Iran, and Europe, respectively. Some studies analyzed the impact of historical/future climate change on BW and GW resources by assuming a constant land use pattern. For instance, Abbaspour et al. (2009) assessed the future impact of climate change on BW and GW in Iran by using Canadian Global Coupled Model (CGCM) and Soil and Water Assessment Tool (SWAT), and Chen et al. (2014) did similar analysis in the large-scale basins in China with the use of Atmosphere-Ocean General Circulation Models (GCMs) and a hydrological model named MPI-HM. Zang and Liu (2013) analyzed the BW and GW trends in the Heihe River Basin in China using historical precipitation data, but no clear relationship between BW and GW trends and climate change was stated.

Although some studies have looked at the spatio-temporal distribution of BW and GW in China with the application of SWAT, they assumed constant land cover over a long historical period, and did not correlate such spatio-temporal pattern to climate and land use change. Zang et al. (2012) assessed the spatio-temporal distribution of BW and GW, but they did not correlate such spatio-temporal pattern to the change of climate and land use. Zuo et al. (2015) analyzed the spatial distribution of BW and GW and their average seasonal patterns by assuming constant land use pattern. Zhang et al. (2014) performed the spatio-temporal analysis of BW and GW in the Headwater of Yellow River Basin, China, but they did not consider land use change.

While other studies focused on the impacts of land use change on BW and GW, they did not explicitly separate the noise of climate variation/change from the impacts of land use change on long-term BW and GW dynamics. For example, Glavan et al. (2013) investigated the influences of the historical land use change over 200 years on BW and GW in two Slovenian Mediterranean catchments by using current climate condition. Jewitt et al. (2004) used two hydrological models, ACRU and HYLUC, to study BW and GW dynamics under nine simulated land use scenarios in the Luvuvhu Catchment, South Africa. Liu et al. (2009) quantified the effects of historical land cover change on BW and GW in Laohahe Catchment in China by using a semi-distributed hydrological model, but the resultant BW and GW changes included climate influences only.

A restricted number of studies attempted to model and quantify the combined and individual influence of climate and land use change, but their outcomes are limited by a

variety of assumptions. For example, Li et al. (2009) quantified the impacts of land use change and climate variability on BW and GW components (runoff, soil water and ET) in Heihe catchment in China, but the 20-year study period was too short to make a conclusion about any climate change. Xu (2013) used the ratio of annual GW to annual precipitation as an index to assess GW under the influence of climate and land use change in a drainage area, but he excluded deep aquifer and root zone soil water contents from GW.

1.3 Research Objectives

Although many studies focused on the BW and GW dynamics, their findings are limited to some extent because they did not separate the relative contributions of climate and land use change to BW and GW. These limitations give less practical value to future water resources prediction and management. Therefore, this study intends to provide a comprehensive understanding about the influence of long-term climate and land use change on the spatio-temporal patterns of BW and GW in a large basin. First, historical climate and variable land use data are employed in the models to simulate BW and GW fluxes closer to reality. Second, in addition to the combined effects of climate and land use change, their individual contributions are quantified by isolating the land use variables from the combined influence. Furthermore, the spatio-temporal analysis helps identify the regions for further focal analysis where BW or GW is sensitive to climate or land use change.

The objectives of this study are to: (1) analyze the spatio-temporal pattern of BW and GW in the study area under historical climate and land use changes from 1935 to 2014 at three levels (the whole basin, region, and sub-basin levels), and (2) quantify the relative contributions of climate change or land use change to BW and GW variability. These objectives are accomplished by choosing Ohio River Basin (ORB) as the study area because of the prominent changes in climate and land use, and its agricultural, industrial and domestic importance. The Soil and Water Assessment Tool (SWAT) is adopted for the hydrologic simulation, and trend analyses are performed using Mann-Kendall and Theil-Sen tests.

1.4 Thesis Organization

This thesis is organized in six chapters. Chapter 1 presents research background, research objectives, and an outline of this thesis. Chapter 2 presents a brief description of study area and the input data for SWAT modeling. Chapter 3 presents the methodology used for hydrologic simulation, statistical analysis, and the separation of climate and land use effects. Chapter 4 presents the results of observed climate and land use change, BW and GW spatio-temporal patterns, and relative contributions of climate and land use effects on BW, GW and their components (total water yield, deep aquifer recharge, ET, and soil water content) in the basin scale. Chapter 5 discusses the results in this study, and attempts to explore the differences within the context of previous studies. The uncertainty and limitation of this study are also discussed in Chapter 5. Chapter 6 presents the summary and conclusions for this study.

CHAPTER 2. STUDY AREA AND DATA INPUT

2.1 Introduction

Since this study focuses on the spatio-temporal impacts of climate and land use change on BW and GW in a large scale basin, the Ohio River Basin (ORB) is used as the study area because of the prominent change in climate and land use. The ORB land use, which consists mainly of agricultural, forest and urban areas, has experienced extensive conversion from agricultural area to forests due to conservation reserve program since the 1940s (Tayyebi et al., 2015). Historical climate data in ORB also shows a significant increasing trend in precipitation.

In addition, ORB has great importance in agricultural, industrial, and domestic water supply. The northwestern portion of ORB is within the Western Corn Belt (WCB), one of the most agriculturally intensive areas of USA, accounting for more than 50% of total corn and soybean production in the country (Schnitkey, 2013). In addition to agriculture, ORB serves drinking water for about 10% of the population and produces about 20% of the electricity for the entire USA. Given that BW is important to domestic and industrial water supply and that GW is essential for agricultural productivity, the evaluation of BW and GW availability under prevalent climate and land use changes in ORB holds great significance.

2.2 Study Area

Ohio River is the largest tributary of Mississippi River by discharge and flows 981 miles from Pittsburgh, Pennsylvania to Cairo, Illinois. The drainage area of ORB is 491,000 km², covering the entire or part of total 11 states (Fig. 2.1). Located between 34°N and 41°N latitude and 77°W and 89°W longitude, ORB's eastern extent lies in the Blue Ridge, Valley and Ridge, and Appalachian Plateaus provinces; the central portion includes the Interior Low Plateaus, and reaches the Coastal Plain province in the west.

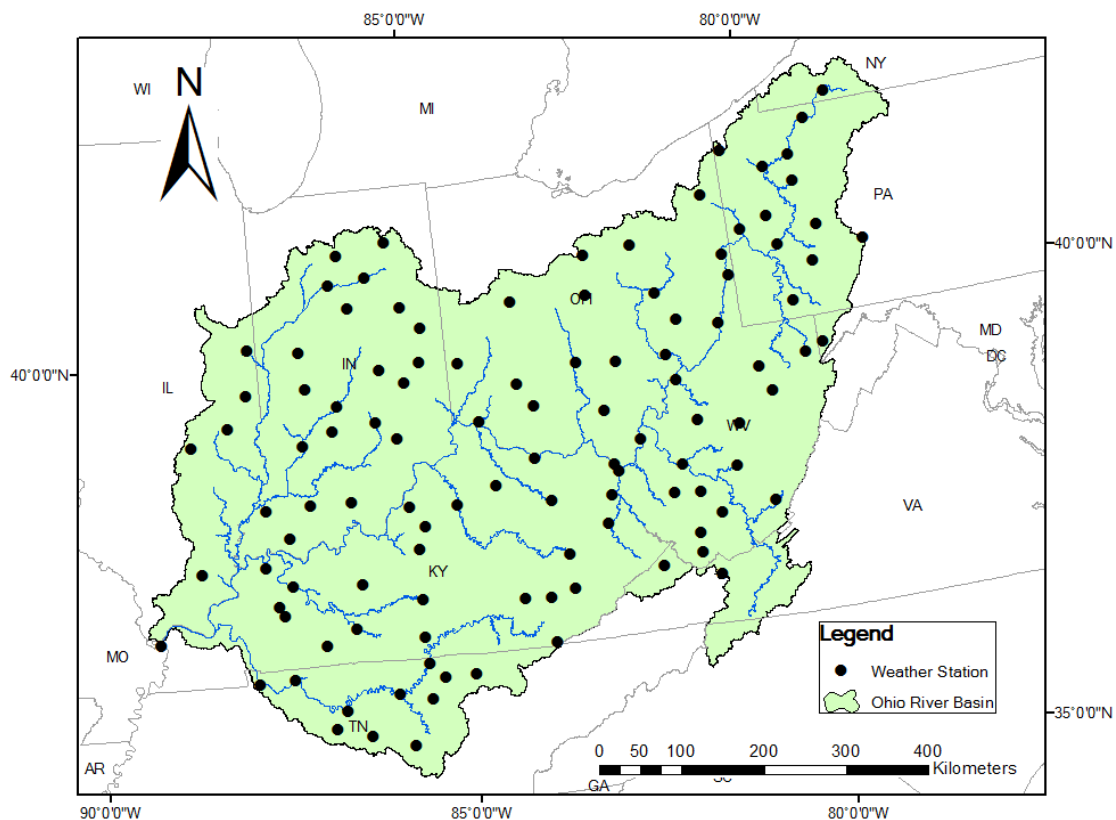


Figure 2.1 Study Area and Weather Station Location

The topography, land use and climate in ORB vary gradually from east to west. The elevation in the ORB ranges from 30 m above sea level in the flat western parts to 1,745 m in the hilly eastern areas, and the elevation in the east is generally higher than that in the west. The slope also increases from the northwest to the southeast. ORB was historically covered by forest, and due to its flat topography and low elevation, the predominant land use in the western parts has been developed into agriculture at the beginning of the study period (1940), while the eastern part remains forestry. However, at the end of the study period (2010), a large portion has been transformed into second-growth forest in response of the conservation reserve program established around 1940 (Tayyebi et al., 2015). Urban area keeps increasing in ORB, but the change in urban area is still relatively small.

The climate of ORB is temperate in the north and humid continental temperate in the southeast (O'Donnell et al., 2000). In winter, the monthly mean temperature varies from -7°C to 10°C and in summer from 24°C to 28°C (White et al., 2005). According to the climate data during the study period (1935-2014), annual precipitation for the entire basin ranges from 840 mm/year to 1484 mm/year. The annual maximum and minimum temperature vary from 16.6°C to 20.0 °C and 2.5°C to 7.3°C, respectively. The annual precipitation increases slightly from the southeast to the northwest due to higher elevations in the southeast. Snow accumulation is significant in the north and Appalachians (White et al., 2005).

2.3 Input Data

Creation of the SWAT models requires topography, soil texture, land use and climate data, and calibration and validation of the SWAT models needs observed streamflow data. Digital elevation model (DEM) data at 30 m spatial resolution is extracted from U.S. Geological Survey's (USGS) National Elevation Dataset (NED). For the soil data, this study uses the 1:250,000 scale State Soil Geographic Data (STATSGO) directly from the SWAT 2012 database. Five historical land use maps, one for each decade during 1935 to 1985, are obtained from the Human-Environment Modeling and Analysis (HEMA) Laboratory, Department of Forestry and Natural Resource at Purdue University (Tayyebi et al., 2015). The historical land use maps have four land cover classes: forest and rangeland, agriculture, urban and other land use (e.g. wetland/barren). For the remaining three decades of the study period (1985-2014), 30 m land use maps are obtained from USGS's National Land Cover Dataset (NLCD) 1992, 2001 and 2011. The original NLCD land use maps are then reclassified into the same classes as in the historical land use maps.

The climate data are obtained from the National Climatic Data Center (NCDC) for 112 weather stations that are nearly uniformly distributed within the basin, providing total daily precipitation, average daily maximum and minimum temperature records which cover the entire period of simulation (Fig.2.1). The other climate components, like solar radiation and relative humidity, are developed through the internal weather generator in SWAT. The weather data for each sub-basin are assigned automatically in SWAT using

the closest weather station. The daily observed streamflow data required for calibration and validation are obtained from USGS's gauge stations (Fig.2.2). There are more than 60,000 USGS gauge stations in ORB, but very few of them have the complete streamflow records from 1935 to 2014. In addition, as this study does not consider reservoir management, many available USGS streamflow gauge stations along the main channel of the Ohio River are not selected in order to minimize the influence of existing dams/locks in model calibration. The site information for calibration and validation is listed in table 2.1.

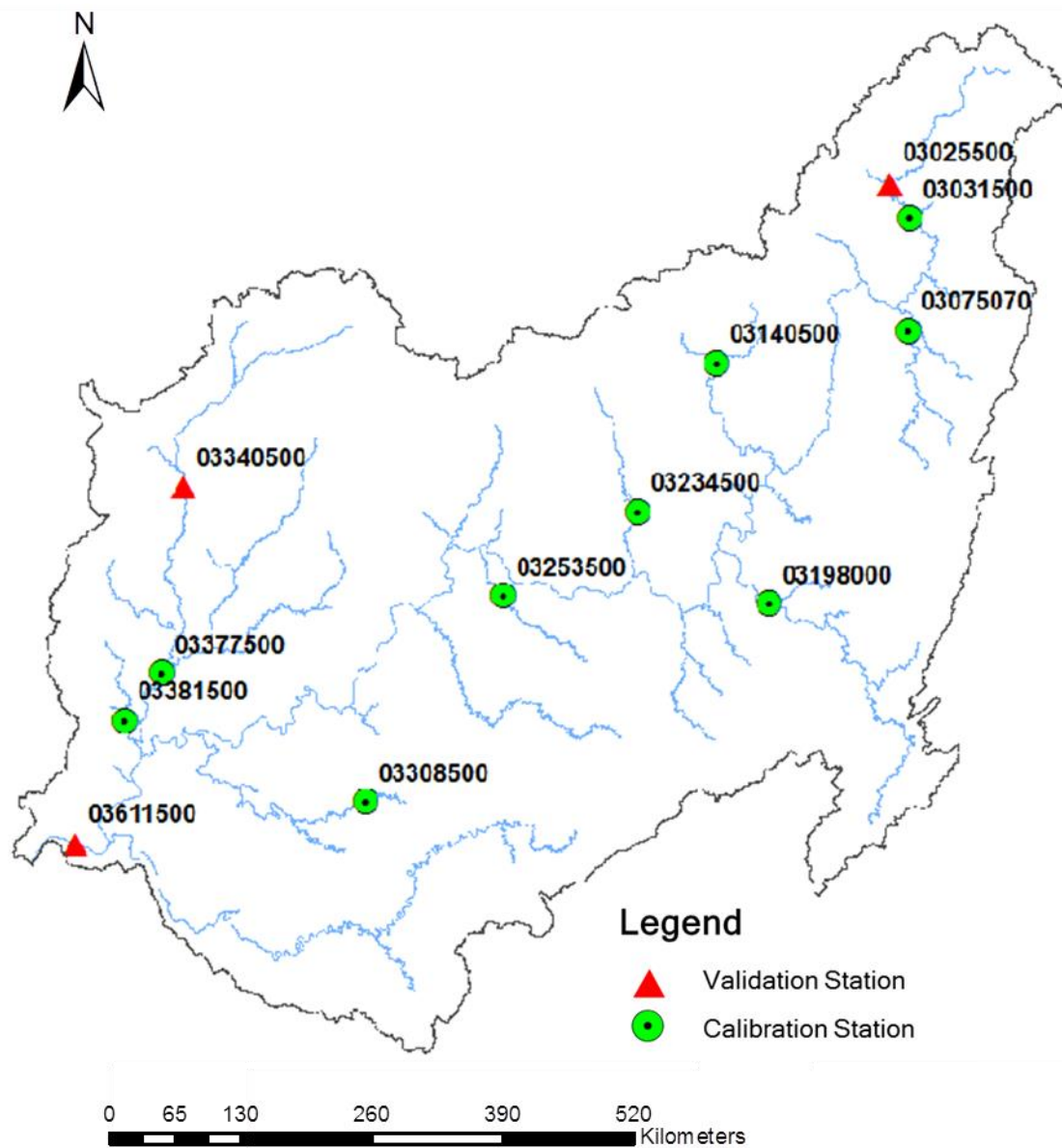


Figure 2.2 Calibration and Validation Station Location

Table 2.1 Calibration and Validation Sites Information

USGS Site Name	Site Number	Latitude	Longitude
ALLEGHENY RIVER AT FRANKLIN, PA	03025500	41°23'22"	79°49'14"
ALLEGHENY RIVER AT PARKER, PA	03031500	41°06'02"	79°40'53"
MONONGAHELA RIVER AT ELIZABETH, PA	03075070	40°15'44"	79°54'05"
MUSKINGUM RIVER NEAR COSHOCTON OH	03140500	40°14'54"	81°52'23"
KANAWHA RIVER AT CHARLESTON, WV	03198000	38°22'17"	81°42'08"
SCIOTO RIVER AT HIGBY, OH	03234500	39°12'44"	82°51'50"
LICKING RIVER AT CATAWBA, KY	03253500	38°42'37"	84°18'39"
GREEN RIVER AT MUNFORDVILLE, KY	03308500	37°16'10"	85°53'17"
WABASH RIVER AT MONTEZUMA, IN	03340500	39°47'33"	87°22'26"
WABASH RIVER AT MT. CARMEL, IL	03377500	38°23'54"	87°45'23"
LITTLE WABASH RIVER AT CARMIL, IL	03381500	38°03'40"	88°09'35"
OHIO RIVER AT METROPOLIS, IL	03611500	37°08'51"	88°44'27"

CHAPTER 3. METHODOLOGY

3.1 Introduction

This chapter presents the methodology for the BW and GW simulation, trend analysis, and quantifying the relative contributions of climate and land use effects. The model mechanism and setup of Soil and Water Assessment Tool (SWAT) are first described in Section 3.2 and 3.3. Sequential Uncertainty Fitting Version 2 (SUFI-2) in SWAT-CUP is used for model calibration and validation. Mann-Kendall test and Theil-Sen approach are used to detect the trend and magnitude of the trend line, respectively. Finally, the method for separating climate and land use effects are briefly described in Section 3.6.

3.2 Model Description

SWAT has been widely used to analyze BW and GW in large-scale basins ($>100,000\text{km}^2$) (Faramarzi et al., 2013; Zang et al., 2012; Zhang et al., 2014; Zuo et al., 2015). SWAT is a semi-distributed, conceptual model to simulate hydrologic and chemical processes in a basin scale over long time scales. SWAT incorporates a number of different physical processes within a watershed, including climate, hydrology, chemical and nutrient transport, sediment transport, land cover and practice management, and water resources management. In this study, SWAT is adopted to simulate hydrologic fluxes because of its

good performance in large-scale models, computational efficiency, and wide-spread application in simulating BW and GW.

In general, SWAT simulates watershed physical processes based on daily water balance in soil content and routing phase through the watershed (Neitsch et al., 2011). The water balance equation in SWAT is presented below (Neitsch et al., 2011):

$$SW_t = SW_0 + \sum_{i=1}^t (R_{day} - Q_{surf} - E_a - w_{seep} - Q_{gw}) \quad \text{Equation 3.1}$$

Where SW_t is the final soil water content (mm H₂O), SW_0 is the initial soil water content on day i (mm H₂O), t is the total number of simulated days, R_{day} is the amount of precipitation on day i (mm H₂O), Q_{surf} is the amount of surface runoff on day i (mmH₂O), E_a is the amount of ET on day i (mm H₂O), w_{seep} is the amount of water entering the vadose zone from the soil profile on day i (mm H₂O), and Q_{gw} is the amount of return flow on day i (mm H₂O).

3.3 Model Setup

This study utilizes the ArcSWAT 2012 interface to set up SWAT for simulating BW and GW fluxes. The original DEM, soil, and land use data are resampled to a 90 meter horizontal resolution to keep the model computational time in ArcSWAT reasonable. The entire ORB is divided into 125 sub-basins by using a flow accumulation threshold of 0.5% basin area (2500 km²). Since ORB has a large drainage area, and in order to keep the

computational time of the models within a practical limit, the sub-basins are not further divided into multiple Hydrologic Response Units (HRUs). Instead, dominant land use, soil type, and slope classes are used to represent the typical geospatial character of a particular sub-basin (Winchell et al., 2010). This leads to the assumption that the simulated hydrologic variable over a particular sub-basin is representative of the average condition of the whole sub-basin. Considering the elevation differences across the basin, the slope is classified into three classes: 0-4%, 4-10%, and >10%. In this study, SCS Curve Number method is selected for surface runoff generation, Penman-Monteith equation is selected to compute potential evapotranspiration (PET), and Variable Storage method is selected for channel routing simulation (Neitsch et al., 2011).

To analyze BW and GW availability due to combined and separated impacts from climate and land use change, two SWAT configurations are created in this study. In the first configuration, eight decadal SWAT models are created using historical climate and land use data to study the combined effects of land use and climate change. This model configuration is named 'variable climate-variable land use' for this study. In this configuration, the study period from 1935 to 2014 is first divided into eight 10-year periods and each SWAT model simulates one of the eight periods by using historical climate and land use data corresponding to that period. For each model, the first year is used as the warm-up period so that the influence of initial condition can be excluded. To separate the impact of climate and land use change, a scenario where the land use remains constant, but climate varies as the historical data is created. This configuration is named

as ‘variable climate-steady land use’ for this study, and this hypothetical model has the input of 1940’s land use and variable weather input over the study time span.

3.4 Tile Drainage

As a predominantly agricultural region, ORB has artificial subsurface drainage (tile drainage) in nearly 30 % of its areas (Jaynes & James, 2007). The function of tile drainage is to maintain the productivity of poorly drained soils. Tile drainage is very important to hydrologic balance because tile drains intercept percolating waters and route them directly to surface waters (Green et al., 2006). Considering the density and importance of tile drainage in ORB, the tile drainage system is simulated in the SWAT model. Most of the tile drainage in the northern part of the United States was installed between 1870 and 1920 and between 1945 and 1960 (Zucker & Brown, 1998). In the absence of information on historical tile drainage installation, tile drains are assumed to be installed for the entire basin at the beginning of the study period, and the percentage of tile drainage keeps constant throughout the study period. Previous studies assumed tile drainage to be installed in ‘somewhat poorly-drained’, ‘poorly-drained’, and ‘very poorly-drained’ soils (Boles, 2013). However, in order to maintain the reported percentage of total drainage area (about 30%), tile drains are only included in the model in agriculture land with ‘poorly-drained’ and ‘very poorly-drained’ soils. In SWAT, four parameters are needed to simulate the tile drains: DEP_IMP, depth to impermeable layer (mm), DDRAIN, depth of surface drain (mm), TDRAIN, time to drain soil to field capacity (hour), and GDRAIN, drain tile lag time (hour). Based on previous studies (Du

et al., 2005; Rahman et al., 2014; Singh et al., 2005), DEP_IMP is set to 1200 for ORB, DDRAIN is set to 1000, TDRAIN is set to 24, and GDRAIN is set to 48.

3.5 Model Calibration, Parameterization, and Validation

3.5.1 Calibration Method

The calibration and validation process is conducted using Sequential Uncertainty Fitting Version 2 (SUFI-2) in SWAT-CUP (Abbaspour, 2013). Rather than specifying a set of best-fit parameters, SUFI-2 aims to find a good parameter range with the view of the uncertainty issues on parameters, including conceptual modeling uncertainty, input uncertainty, and parameter uncertainty. SUFI-2 adopts two indicators to measure the goodness of model performance: P factor and R factor (Abbaspour et al., 2004). P factor refers to the percentage of measured data within the 95% prediction uncertainty (95PPU) band of the cumulative output distribution. R factor is the ratio of the 95PPU band width to the standard deviation, or the “thickness” of the 95PPU envelop. The range of P factor is 0 to 1, and the higher P factor is, the more observed data is bracketed in the 95PPU. In general, a well calibrated model should bracket most of the observed data and has a narrow prediction uncertainty band. Abbaspour et al. (2015) suggest that P factor > 0.75 and R factor < 1.5 is adequate for discharge.

In this study, the Kling-Gupta Efficiency (KGE) (Gupta et al., 2009; Kling et al., 2012) is used as the objective function to evaluate the goodness of model performance. The KGE function is defined as (Gupta et al., 2009):

$$KGE = 1 - \sqrt{(r - 1)^2 + (\beta - 1)^2 + (\gamma - 1)^2} \quad \text{Equation 3.2}$$

$$\beta = \mu_s / \mu_o \quad \text{Equation 3.3}$$

$$\gamma = \frac{\sigma_s / \mu_s}{\sigma_o / \mu_o} \quad \text{Equation 3.4}$$

Where r is the linear regression coefficient between the simulated and observed value, μ is the mean value, σ is the standard deviation, and s and o denotes simulated and observed values, respectively.

As multiple gauge stations are adopted for calibration/validation, the agreement between observed and simulated data for the entire basin is estimated following the approach shown by Abbaspour et al. (2015):

$$KGE' = \sum_{i=1}^n w_i (KGE_i) \quad \text{Equation 3.5}$$

Where i denotes the streamflow gauge stations used in calibration and w is the weight assigned for each station; n is the total number of gauge stations involved in the observation datasets. Thus, KGE calculated for individual sets of observed and simulated streamflow hydrographs are aggregated into KGE' and it is maximized towards an optimal solution. Here, equal weights are assigned to every gauge station ($w_i = 1/n$). The assignment of weights is subjective, and it may affect the outcome of the optimization exercise by SUFI-2. In addition to KGE, Nash Sutcliffe Efficiency (NSE) and Percent

Bias (PBIAS) are also calculated to evaluate the goodness-of-fit between the observed and simulated streamflow.

3.5.2 Calibration Procedure

This study uses a general approach to calibrate large-scale distributed models (Abbaspour et al., 2015). The models are first built by ArcSWAT with different sets of data input and then run without any calibration. The default model outputs are then compared with the observed data by KGE (Table 3.1). KGE' ranges from 0.43 to 0.55 for uncalibrated decadal models, and the results suggest a mediocre performance by the default models. Given the performance of the default models, it is necessary to calibrate the models using SUFI-2.

The daily streamflow observed data of nine USGS gauge stations from 1935 to 2014, which are uniformly distributed in ORB, are used for model calibration. For the eight models simulating 'variable climate-variable land use', the first year is chosen as the warm-up period, and the remaining nine years is used for calibration. For the 'variable climate-steady land use' configuration, the model is calibrated for 1935-1944 with a five year warm-up period (1935-1939), and then the parameters are manually adjusted for a better match of the observed streamflow over 80 years (1935-2014).

Table 3.1 KGE for Uncalibrated Models

Calibration Location	Model Period							
	1935-1944	1945-1954	1955-1964	1965-1974	1975-1984	1985-1994	1995-2004	2005-2014
3031500	0.29	0.32	0.24	0.31	0.32	0.36	0.55	0.44
3140500	0.42	0.7	0.64	0.53	0.61	0.62	0.69	0.6
3075070	0.49	0.62	0.6	0.66	0.62	0.61	0.62	0.59
3234500	0.32	0.25	0.1	0.09	0.05	0.21	0.27	0.6
3198000	0.62	0.46	0.42	0.39	0.35	0.41	0.61	0.46
3253500	0.36	0.39	0.29	0.26	0.33	0.45	0.35	0.4
3377500	0.68	0.79	0.75	0.72	0.69	0.72	0.72	0.74
3381500	0.44	0.79	0.6	0.56	0.56	0.6	0.51	0.65
3308500	0.29	0.32	0.3	0.44	0.56	0.48	0.52	0.46
KGE'	0.43	0.52	0.44	0.44	0.45	0.50	0.54	0.55

Before the calibration starts, a total number of 14 parameters is selected, involving surface, subsurface, and channel hydrologic responses. The initial ranges for these parameters are shown in Table 3.2. The selection of parameters and their initial ranges are based on the review of existing literature and prior knowledge of the study area (Kumar et al., 2009; Larose et al., 2007; Rajib & Merwade, 2015), as well as suggestions from model developers (Abbaspour et al., 2015; Neitsch et al., 2011).

After the parameters and ranges are selected, a maximum of three batch iterations (500 iterations for each batch) are executed to find the best set of parameters which maximize the objective function (KGE in this study). After each set of iteration, the parameter range is narrowed to their best values. Then, successive iterations are performed by taking the updated parameter range from the previous iteration as input.

Table 3.2 SWAT Calibration Parameters

No.	Parameter Name	Description ¹	Scale of Variation	Adjustment ²	Initial Range
1	CN2	Curve Number, moisture condition II	HRU	x	-0.2 – 0.2
2	CH_K2	Channel Hydraulic Conductivity, mm/hr	Watershed	=	5.0 – 100.0
3	CH_N2	Main Channel Manning's n	Watershed	=	1.01– 0.15
4	CANMX	Maximum Canopy Storage, mm	HRU	=	0.0 – 25.0
5	SURLAG	Surface Runoff Lag Coefficient, days	Watershed	=	0.05 – 24.0
6	ESCO	Soil Evaporation Compensation Factor	HRU	=	0.01 – 1.0
7	EPCO	Plant Uptake Compensation Factor	HRU	=	0.01 – 1.0

¹ Source: Neitsch et al. (2011)

² Type of change applied over the existing parameter value: 'x' means the original value is multiplied by the adjustment factor, '=' means the original value is replaced by a value from the range, '+' means a value from the range is added to the original value.

8	SOL_AWC	Available Soil Water Capacity, mmH ₂ O per mm of soil	HRU	x	-0.15 – 0.15
9	SOL_K	Saturated Hydraulic Conductivity, mm/hr	HRU	x	-0.15 – 0.15
10	ALPHA_BF	Baseflow Recession Constant, days	Watershed	=	1.01– 1.0
11	REVAPMN	Re-evaporation (Upward Diffusion) Threshold, mm	Watershed	=	0.01 – 500.0
12	GW_DELAY	Groundwater Delay, days	Watershed	+	-10.0 – 10.0
13	GWQMN	Threshold Groundwater Depth for Return Flow, mm	Watershed	=	0.01 – 5000.0
14	GW_REVAP	Groundwater Re-evaporation Coefficient	Watershed	=	0.02 – 0.2

3.6 Trend Analysis

This study uses the Mann-Kendall test (MK; Mann (1945) and Kendall (1948)) to detect the monotonic trends of simulated data. Based on the MK result, the Theil-Sen approach (TS; Sen (1968)) is used to determine the slope of the trend line.

3.6.1 Mann-Kendall Test

MK is a rank based, nonparametric trend test popular in both hydrologic and climatologic studies (Hamed, 2009; Hamed & Rao, 1998; Lettenmaier et al., 1994). MK does not require the data to follow a specific statistical distribution, which may not always hold

true for hydrologic or climate time series. Therefore, MK is used in the study to detect the trends in simulated annual average values of precipitation, temperature, BW and GW. Hydro-climatic time series often have significant serial correlations (autocorrelations), and thus will affect the accuracy of MK results. For example, positive serial correlation in a time series increases the probability for MK to detect a significant trend (Von Storch, 1999; Yue et al., 2002). Therefore, apart from the classical MK, three modified MK tests are commonly used in trend analysis (Kumar et al., 2009). In MK test with trend-free pre-whitening method (Yue et al., 2002), the time series is judged whether to pre-whiten or not by the lag-one autocorrelation coefficient. If the autocorrelation exists, the time series is detrended using non-parametric TS slope. The second modified MK test considers all the significant autocorrelation structures in a time series, and a modified variance is used to calculate MK statistics (Hamed & Rao, 1998). The last modified MK test, including the presence of long term persistence (Hurst phenomenon), uses a modified variance which is obtained from Hurst coefficient to calculate MK statistics (Hamed, 2008).

Before performing the MK test, tests about autocorrelation and partial autocorrelation coefficient versus lag time on BW, GW, temperature, and precipitation time series are first computed (Fig. 3.1; Fig. 3.2; Fig. 3.3; Fig. 3.4; Fig. 3.5). As most of the vertical spikes in Figures 3.1-3.5 are within the horizontal band for the time series, the influence of serial correlation is not significant, so the classical MK test is selected in this study.

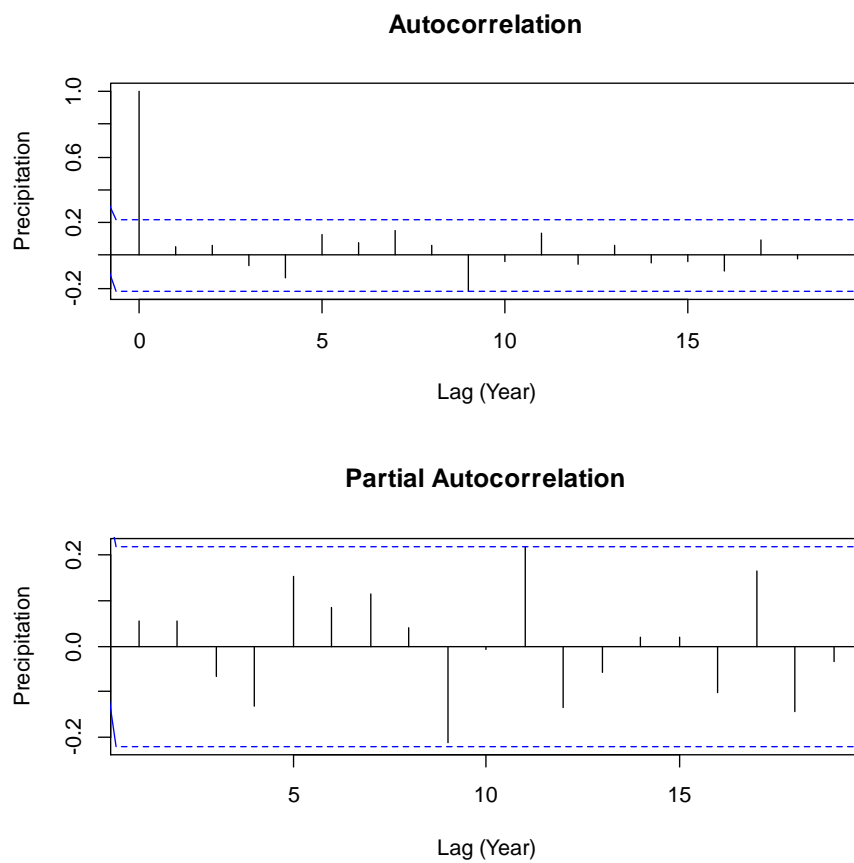


Figure 3.1 Autocorrelation for Annual Precipitation

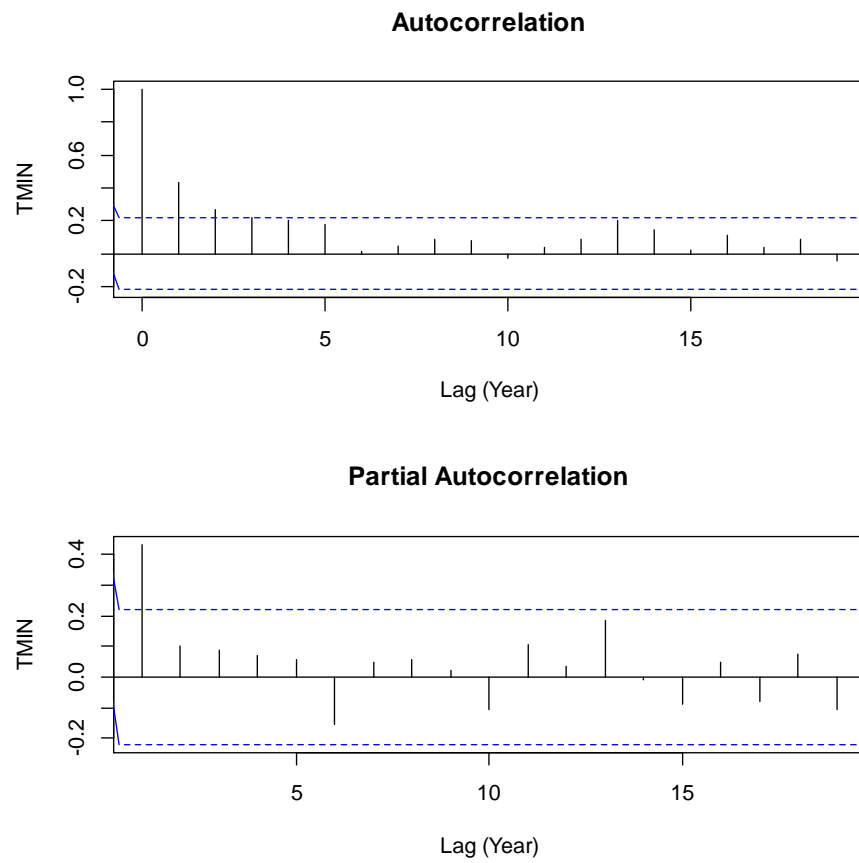


Figure 3.2 Autocorrelation for Annual Minimum Temperature

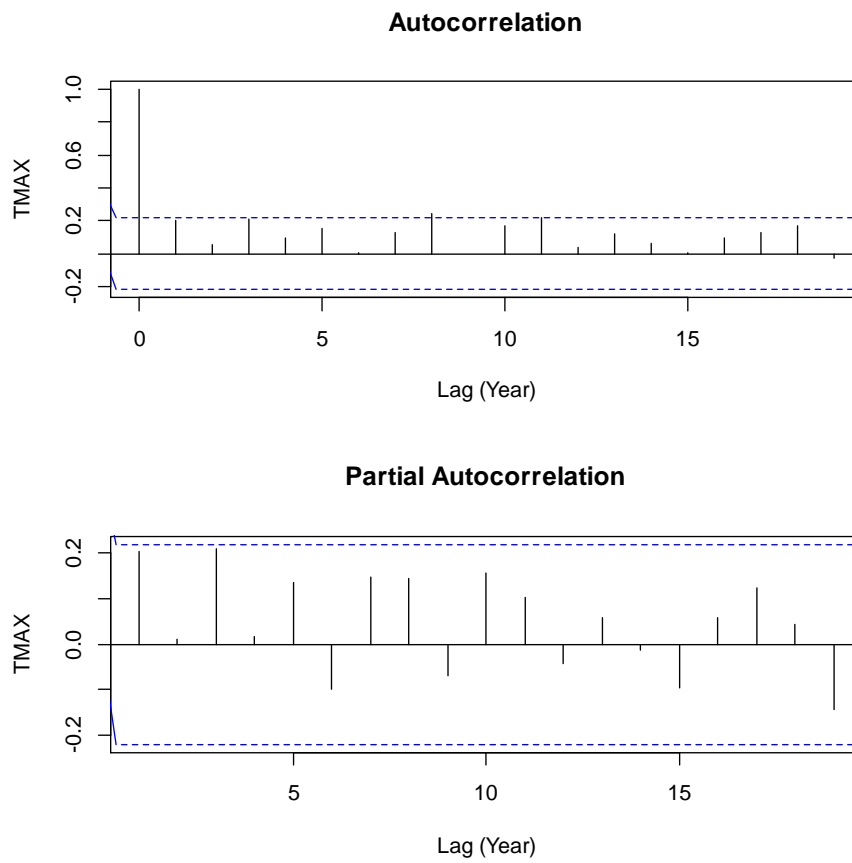


Figure 3.3 Autocorrelation for Annual Maximum Temperature

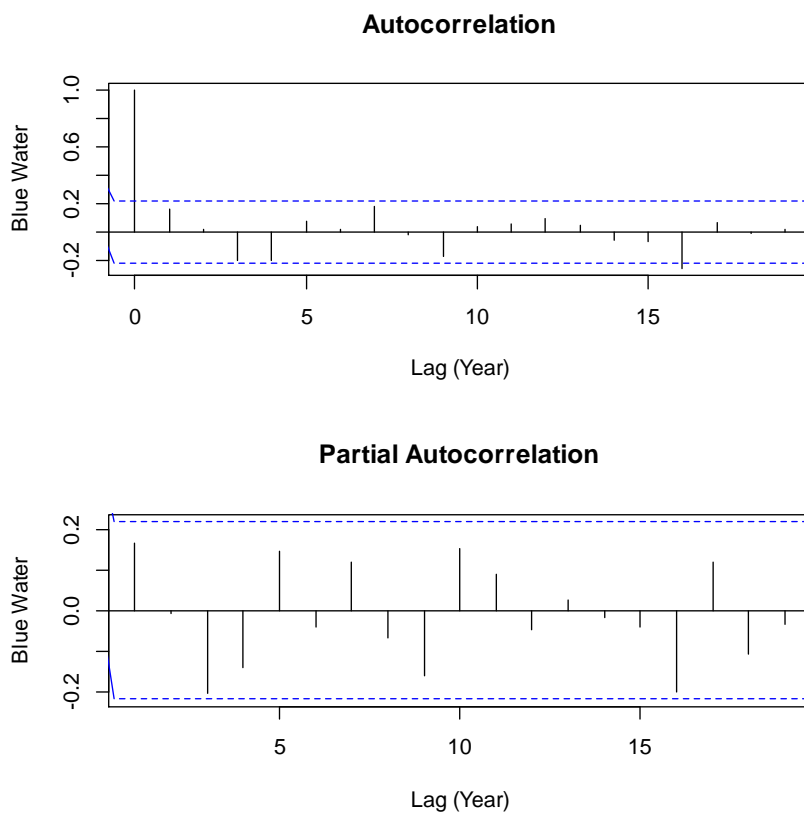


Figure 3.4 Autocorrelation for BW

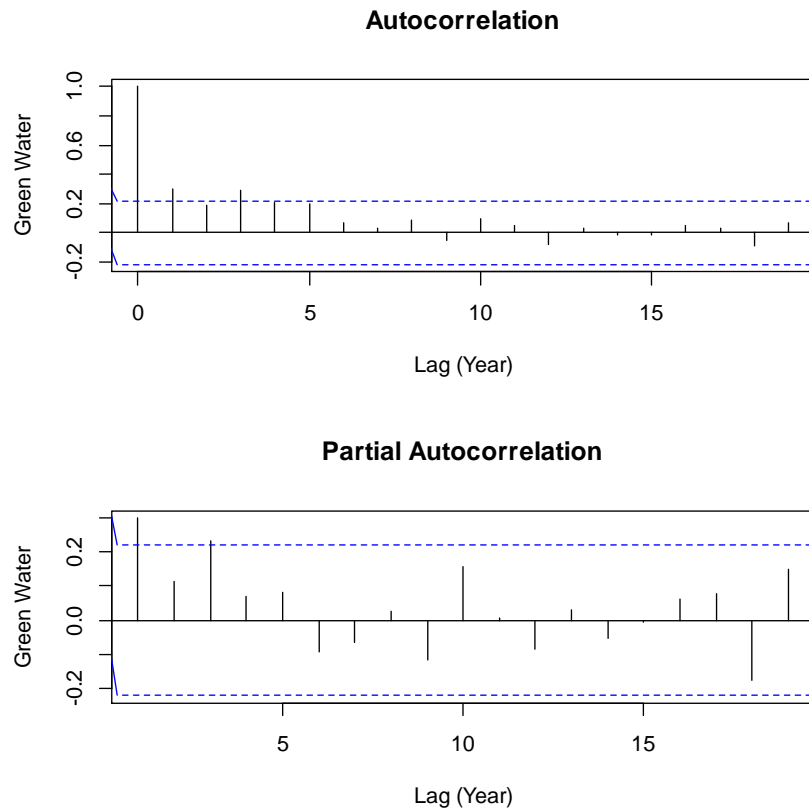


Figure 3.5 Autocorrelation for GW

In the classical MK test, the MK test statistic S and τ for a time series can be calculated as follows (Kendall & Gibbons, 1990):

$$S = \sum_{i=1}^{n-1} \sum_{j=i+1}^n \text{sgn}(x_j - x_i) \quad \text{Equation 3.1}$$

$$\tau = \frac{S}{\frac{1}{2}n(n-1)} \quad \text{Equation 3.2}$$

Where

$$\text{sgn}(x_j - x_i) = \begin{cases} 1 & x_j > x_i \\ 0 & x_j = x_i \\ -1 & x_j < x_i \end{cases} \quad \text{Equation 3.3}$$

x is the observation data in a time series.

In MK test, the null hypothesis is that no trend exists in the time series. MK statistics S or τ indicate the direction of the trend: a positive value indicates an increasing trend and vice versa. The p value indicates the significance level to reject the null hypothesis. In order to interpret the results from MK test, three significance level criteria are used based on p -values, including (i) $p > 0.1$, (ii) $0.1 > p > 0.01$ and (iii) $p < 0.01$, respectively, to signify the trend as not significant (NS), significant (S) and very significant (VS).

3.6.2 Theil-Sen Test

The TS approach is a non-parametric regression method based on the MK statistic, and the slope determined by TS is an estimator of the magnitude of trends. In this study, TS is used to estimate the total changes in precipitation, temperatures, BW, and GW. The upper and lower bound of 95% confidence interval in TS is also calculated to evaluate the coverage of slope. The TS slope β is calculated by:

$$\beta = \text{median} \left[\frac{x_j - x_i}{j - i} \right] \quad \text{for all } i < j \quad \text{Equation 3.4}$$

3.7 Separation of Climate and Land Use Change Impacts

The relative impacts of climate and land use change on BW and GW are quantified using an approach similar to the one proposed by Li et al. (2015). This approach is based on

three assumptions: (1) climate and land use changes are the only two factors affecting the spatio-temporal trends in BW and GW, (2) climate and land surface processes are independent, and (3) in the SWAT model, constant land use and variable climate data do not influence the sensitivity and uncertainties of SWAT parameters. Based on the outputs from the first configuration of ‘variable climate-variable land use’, the differences of average annual values in BW and GW between two discrete periods can be expressed by the following equations:

$$\Delta BW = BW_{2014} - BW_{1935} \quad \text{Equation 3.5}$$

$$\Delta GW = GW_{2014} - GW_{1935} \quad \text{Equation 3.6}$$

Where ΔGW and ΔBW are the total change of GW and BW between initial and final year responding to both climate and land use change; indices 1935 and 2014 correspond to the initial (1935) and final (2014) year of comparison.

By using the second configuration of ‘variable climate-steady land use’, the change in average annual BW and GW due to climate change ($\Delta BW_C / \Delta GW_C$) can be calculated by the following equations:

$$\Delta BW_C = BW'_{2014} - BW'_{1935} \quad \text{Equation 3.7}$$

$$\Delta GW_C = GW'_{2014} - GW'_{1935} \quad \text{Equation 3.8}$$

Where BW' and GW' represent the average annual BW and GW values under the configuration of 'variable climate-steady land use'; indices 1935 and 2014 correspond to the initial (1935) and final (2014) year of comparison.

By comparing the BW and GW changes between the first and second configuration, the change values of BW and GW due to land use change ($\Delta BW_L/\Delta GW_L$) can be obtained by the following equations:

$$\Delta BW_L = \Delta BW - \Delta BW_C \quad \text{Equation 3.9}$$

$$\Delta GW_L = \Delta GW - \Delta GW_C \quad \text{Equation 3.10}$$

Thus the relative contributions of climate and land use impacts on BW and GW change can be obtained by the following equations:

$$\varphi_{bc} = \Delta BW_C / (|\Delta BW_C| + |\Delta BW_L|) \quad \text{Equation 3.11}$$

$$\varphi_{gc} = \Delta GW_C / (|\Delta GW_C| + |\Delta GW_L|) \quad \text{Equation 3.12}$$

$$\varphi_{bL} = \Delta BW_L / (|\Delta BW_C| + |\Delta BW_L|) \quad \text{Equation 3.13}$$

$$\varphi_{gL} = \Delta GW_L / (|\Delta GW_C| + |\Delta GW_L|) \quad \text{Equation 3.14}$$

Where φ_{bc} and φ_{gc} are the percentage of BW and GW change due to climate change, respectively, and φ_{bL} and φ_{gL} are the percentage of BW and GW change due to land use change, respectively.

CHAPTER 4. RESULTS

4.1 Introduction

In this chapter, a general assessment of climate and land use change in ORB is first presented based on historical climate and land use data during the 80 year study period (1935-2014). With the evaluation of calibrated model performance against observed streamflow data, the spatio-temporal trends of BW and GW change under ‘variable climate-variable land use’ configuration are presented at the basin, regional, and sub-basin levels. Finally, the relative contributions of climate and land use change to BW and GW are evaluated by comparing the ‘variable climate-variable land use’ configuration and the ‘variable climate-steady land use’ configuration.

4.2 Land Use and Climate Change

4.2.1 Land Use Change

Figure 4.1 shows the percentage of land use change from both historical and dominant land use maps between 1935 and 2014 in ORB. The 1940’s historical land map shows that agriculture covered 55% of areas in the ORB, while forest and urban area covered 35% and 7% of the area, respectively. By the 2010’s, the percentage of agriculture decreased to 37%, while the portion of forest and urban area increased to 51% and 10%, respectively. The urban area has increased from 7% to 10%, which is relatively small compared to the change in forest area, which has increased by

16%. Therefore, the influence of urban change on BW and GW can be considered negligible compared to that from the increase in forest cover, and the overall land use change impact on BW and GW in ORB can be considered as the conversion of land from agriculture to forest. Compared with the historical land use maps, the portion of forest area at the end of the study period in SWAT dominant land use and the portion of agriculture area at the beginning of the study period are higher. Meanwhile, the portion of urban area in SWAT dominant land use is lower throughout the simulation period. Nevertheless, the dominant land use maps in SWAT have the same trends of decreasing agriculture area, increasing forest area, and negligible urban area change.

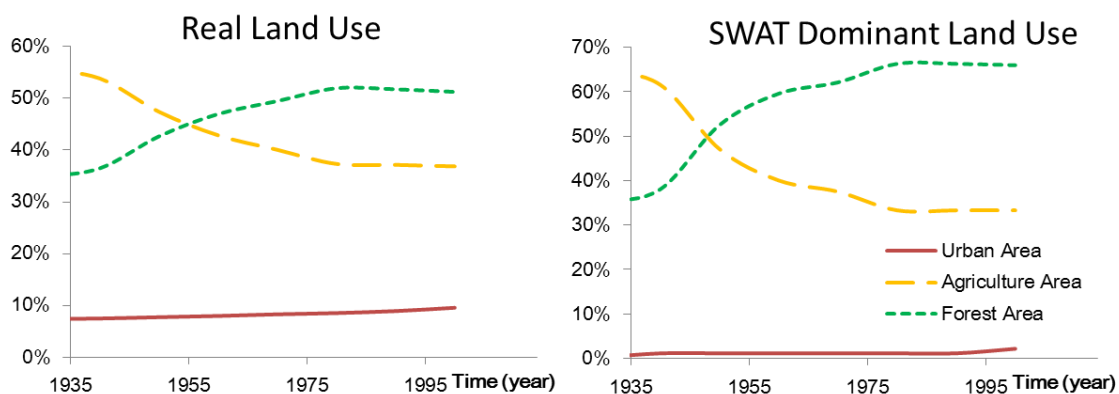


Figure 4.1 Percentage of Land Use from Historical and SWAT Maps

Figure 4.2 shows the change of dominant land use in SWAT throughout the study period. In the 1940's, as the major type of land use, most agricultural sub-basins were in the northwest. In the next few decades, the proportions of both forest and urban land increased by partially replacing the agricultural areas. Specifically, the forest cover

expanded from the southeast to the center of the basin. Overall, nearly one third of the sub-basins in ORB have experienced land use change throughout the study period, most of which occurred in the northeast and southwest regions along the Ohio River.

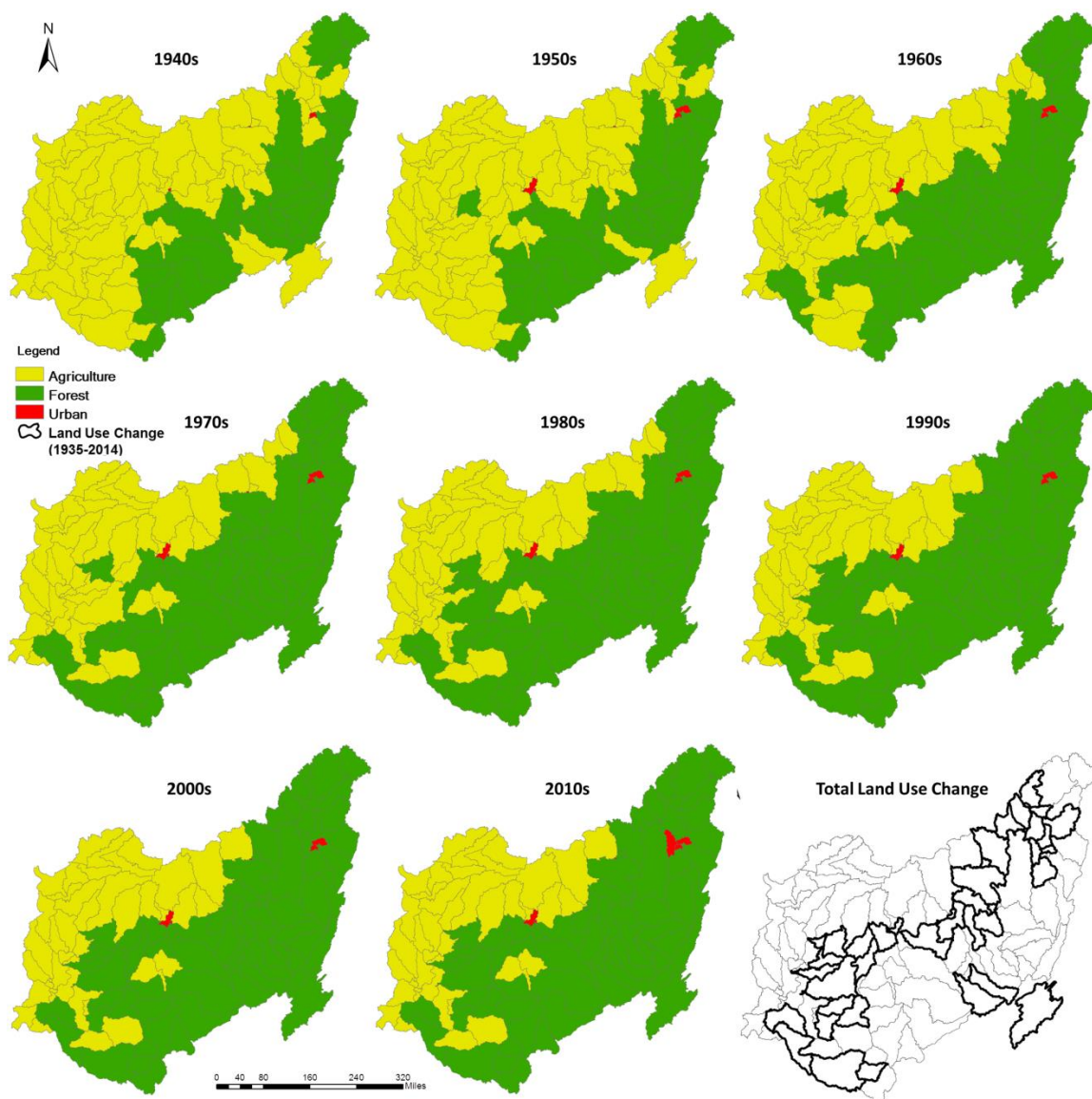


Figure 4.2 Land Use Maps from 1940s to 2010s

4.2.2 Climate Change

The average annual precipitation for ORB shows a significant increasing trend through MK test (Figure 4.3). Accordingly, the average annual precipitation, as estimated by TS test, has increased by 78.1 mm from 1935 to 2014, which means that the precipitation in 2014 is about 8% higher than that in 1935 (Table 4.1). Nevertheless, prominent fluctuations from the trend line throughout the study period are indicative of persistent climate variability in ORB.

Table 4.1 Climate Change Based on TS Result with 95% Confidence Interval

	Precipitation (mm)	TMAX (°C)	TMIN (°C)
Change Based on TS Slope	78.1	-1	0.4
95% Confidence Interval	(42.0,118.2)	(-0.7,-1.3)	(0.2,0.7)

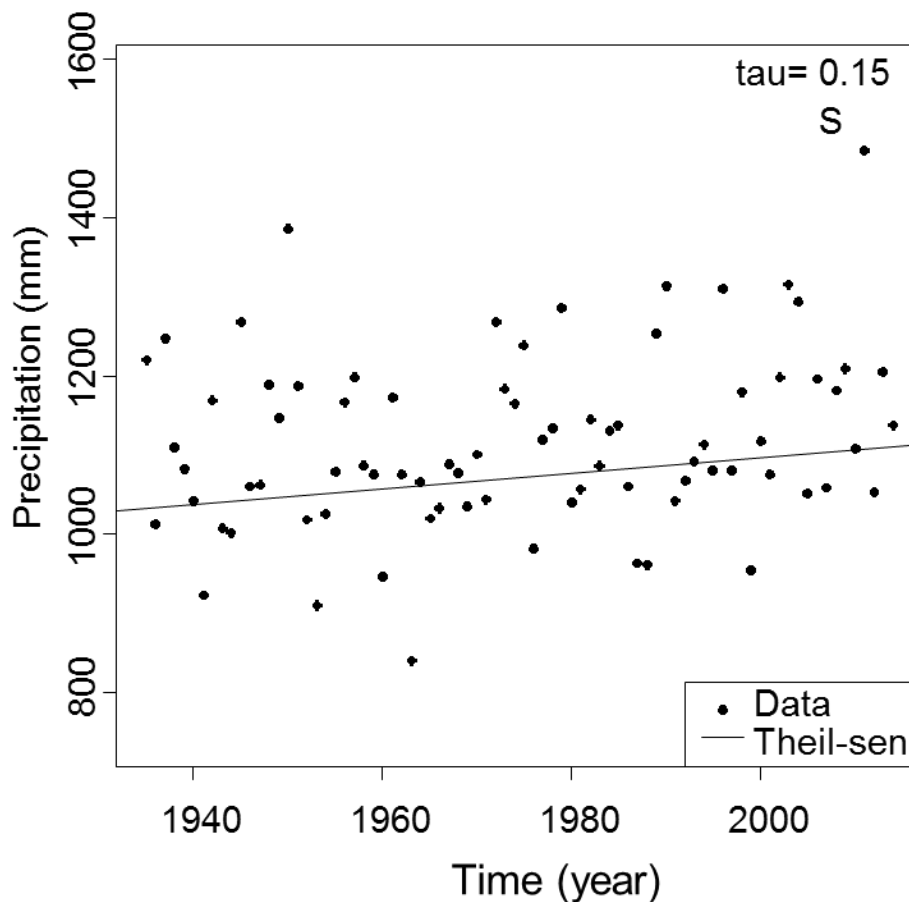


Figure 4.3 MK Test for the Average Annual Precipitation³ (mm yr⁻¹)

As for temperature, average TS slope shows the annual maximum temperature has dropped by 1 °C from 1935 to 2014, while the annual minimum temperature has increased by 0.4 °C (Figure 4.4; Table 4.1). The decreasing annual maximum temperature and increasing annual minimum temperature indicates that the day time is cooler and the night time is warmer in ORB. Despite a narrower fluctuation between maximum and minimum temperature, no clear trend is visible in daily average temperature. An absence

³ Tau is the Kendall rank correlation coefficient (τ). NS means not significant in MK test; S means significant at $p < 0.1$; VS means significant at $p < 0.01$.

of trend in daily average temperature suggests that the primary effect of climate on the hydrologic processes in ORB is due to the significant increasing trend in precipitation.

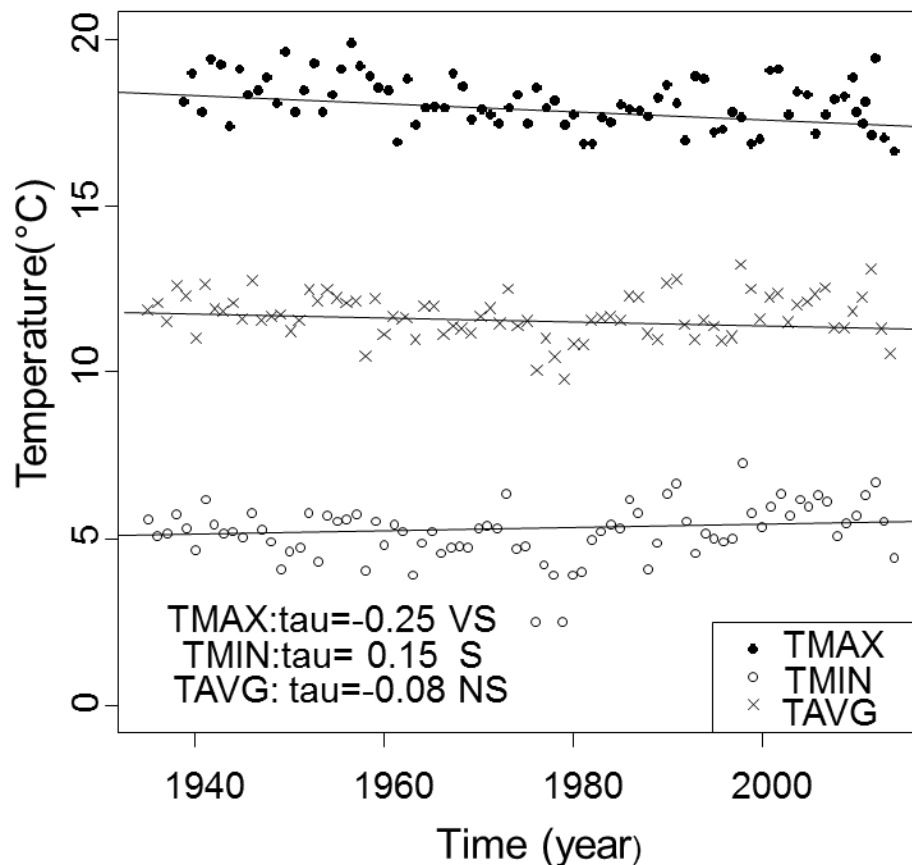


Figure 4.4 MK Test for Annual Maximum, Mean, and Minimum Temperature⁴

The spatio-temporal pattern of annual precipitation in each sub-basin is obtained by comparing the average value in the last thirty years of study period (1985-2014) to that in the first thirty years (1935-1964) (Fig. 4.5). Overall, the precipitation has increased remarkably in most sub-basins, which is analogous to the overall precipitation increase in

⁴ Tau is the Kendall rank correlation coefficient (τ). NS means not significant in MK test; S means significant at $p < 0.01$; VS means significant at $p < 0.1$.

the entire basin. Specifically, the precipitation has increased notably in the whole northwest and in most of the northeast, while a slight decrease in the middle and southern regions is also noticeable.

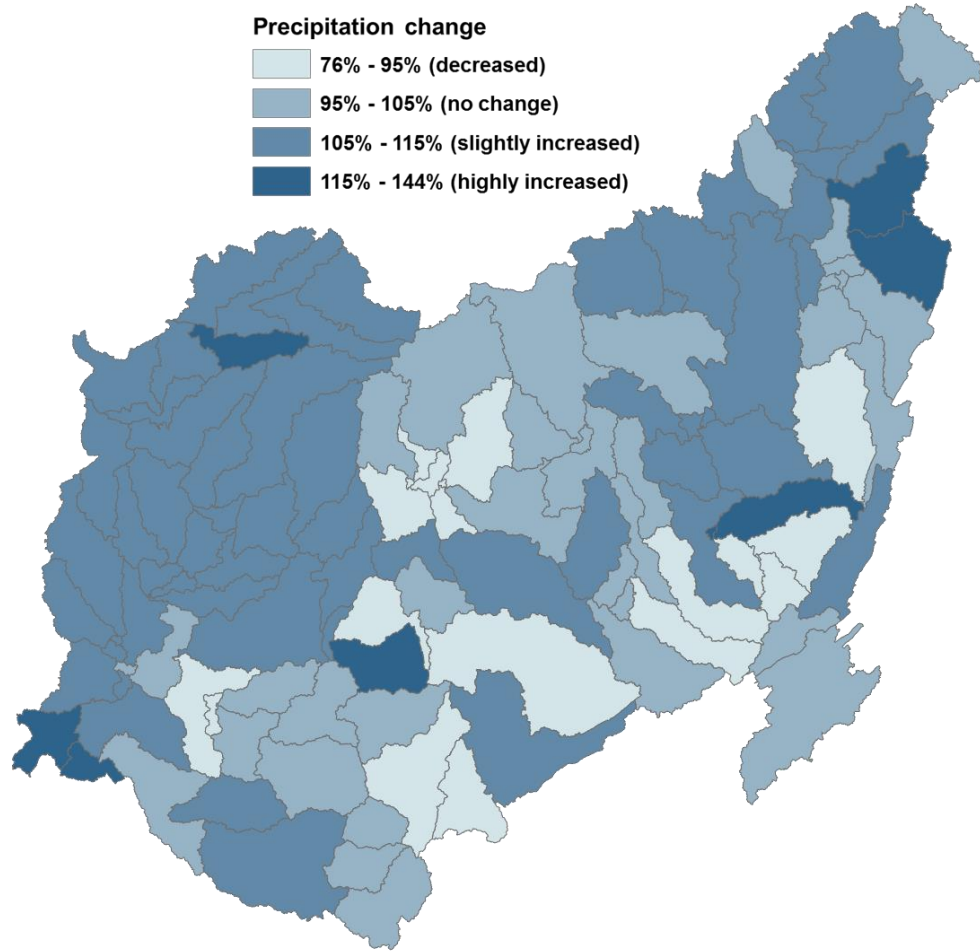


Figure 4.5 Annual Precipitation Change in Sub-basin Scale

4.2.3 Regional Characterization

Based on the spatial characterization of sub-basin scale land use and precipitation distribution shown in Figures 4.2 and 4.5, the entire basin can be divided into three

regions: upper, middle, and lower (Fig. 4.6). This figure identifies the sub-basins which have experienced either land use or precipitation change or both. In general, the land use change in the both upper and lower regions is substantial, while the precipitation increase in the lower region is relatively extensive than that in the upper region. On the contrary, neither land use nor precipitation change can be generalized in the middle region. Details of land use and climate changes in regional scale are shown in Table 4.2, validating the rationale behind this regional sub-division of the ORB.

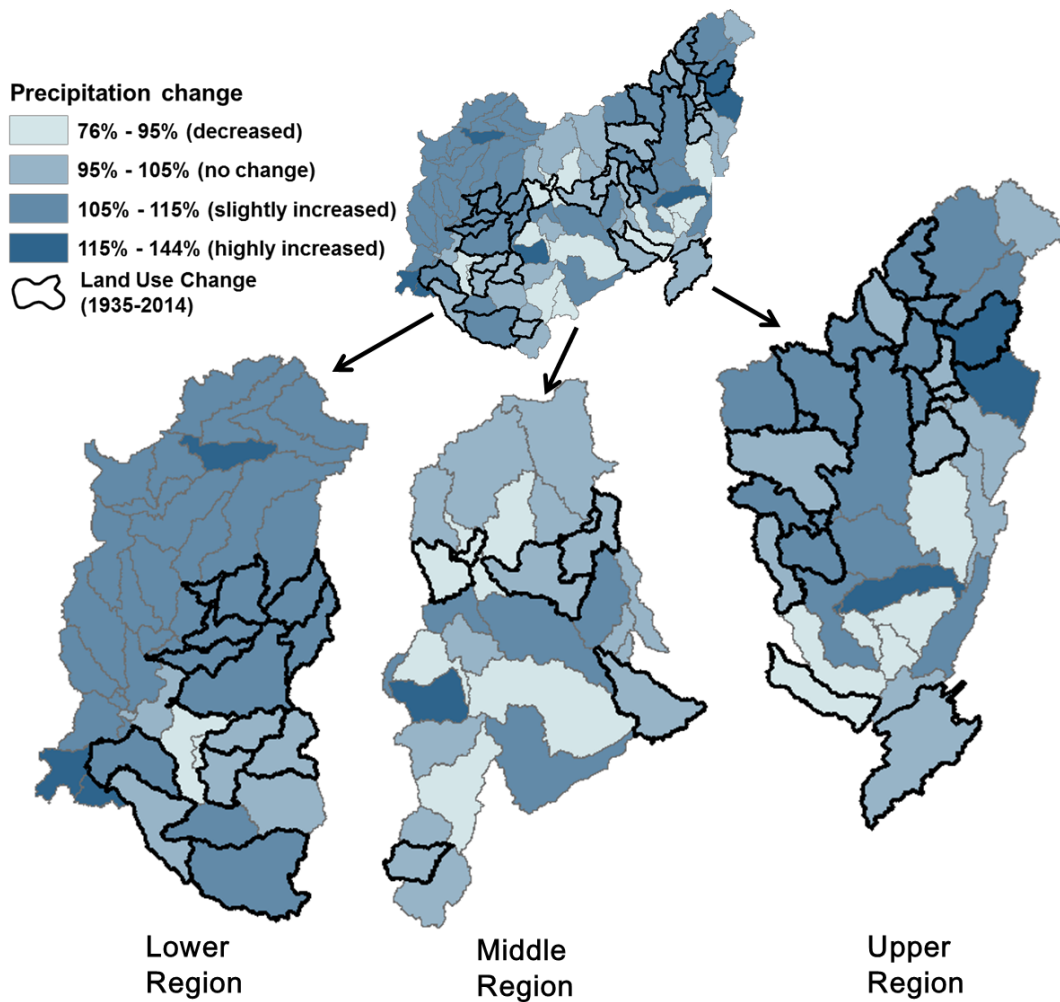


Figure 4.6 Regional Division Based on Climate and Land Use Change

Table 4.2 Regional Comparison of Climate and Land Use Change in ORB

		Upper region	Middle Region	Lower Region
Land use change⁵		41%	15%	35%
Precipitation change	Decreased	15%	29%	3%
	No change	29%	48%	16%
	Slightly increased	46%	19%	78%
	Highly increased	9%	3%	4%

4.3 Model Evaluation

As mentioned in section 3.4, the simulated daily streamflow is compared with the observed data at nine gauge stations for model calibration, and another three gauge stations for validation (Fig. 2.2). The goodness-of-fit scores (KGE, NSE and PBIAS) from calibration and validation under the configuration of ‘variable climate-variable land use’ from 1935 to 2014 are summarized in Table 4.3. Comparing the goodness-of-fit scores (KGE) between calibrated and uncalibrated models from 1935 to 2014, KGE has increased from 0.48 to 0.63 (Table 4.4) after calibration. Except for Site 3075070, where KGE score decreases from 0.60 in uncalibrated models to 0.55 in calibrated models, KGE scores have increased in all other sites. In general, the performance of SWAT models is

⁵ Indicates "any" change in land use that took place during 1935-2014 (example: agriculture transforming into forest, urban or vice versa).

fairly satisfactory for ORB, except for a few high flow events, which can be attributed to the limitation of SWAT in simulating high flows (Kumar et al., 2009; Rajib & Merwade, 2015). Furthermore, as this study focuses more on annual average flows rather than peak/low flows, SWAT simulated results are sufficient for further analysis. Table 4.5 provides the optimized parameter values for all models in this study.

Table 4.3 Goodness-of-Fit Scores for Calibration and Validation Sites

Calibration locations	KGE	NSE	PBIAS
3031500	0.63	0.66	-16
3075070	0.55	0.53	-12
3140500	0.72	0.63	-6
3198000	0.54	0.51	-9
3234500	0.71	0.5	8
3253500	0.48	0.39	3
3308500	0.54	0.45	-16
3377500	0.85	0.79	1
3381500	0.65	0.69	6
Validation locations			
3340500	0.69	0.6	-7
3025500	0.54	0.48	-15
3611500	0.75	0.76	-8

Table 4.4 Comparison of KGE between Uncalibrated and Calibrated Models

Location	KGE	
	Uncalibrated Models	Calibrated Models
3031500	0.35	0.63
3075070	0.60	0.55
3140500	0.60	0.72
3198000	0.47	0.54
3234500	0.24	0.71
3253500	0.35	0.48
3308500	0.42	0.54
3377500	0.73	0.85
3381500	0.59	0.65
Overall	0.48	0.63

Table 4.5 Best Estimates of Calibrated Parameters

Parameter	Best parameter estimates							
	1935-1944	1945-1954	1955-1964	1965-1974	1975-1984	1985-1994	1995-2004	2005-2014
CN2	0.03	0.04	-0.02	0.06	0.04	0.05	0.03	0.04
CH_K2	39.2	84.16	39.67	49.02	84.15	85.3	51.94	53.5
CH_N2	0.03	0.15	0.07	0.04	0.15	0.15	0.12	0.13
CANMX	1.67	14.13	10.63	7.08	14.12	14.12	14.69	14.69
SURLAG	13.07	12.76	12.08	12.25	12.76	12.76	17.89	17.89
ESCO	0.69	0.88	0.86	0.94	0.88	0.96	0.76	0.76
EPCO	0.17	0.46	0.55	0.4	0.46	0.34	0.44	0.44
OV_N	-0.004	-0.06	-0.08	-0.002	-0.06	-0.07	-0.06	-0.06
SOL_K	-0.04	0.07	-0.05	0.03	0.07	0.07	0.11	0.11
ALPHA_BF	0.63	0.62	0.55	0.73	0.62	0.65	0.79	0.79
REVAPMN	116.11	366	170.01	141.31	366	187.75	133.6	133.61
GW_DELAY	-1.34	-4.43	4.15	-4.57	-4.43	-4.5	-3.01	-3.01
GWQMN	232.01	1002.5	82.5	400.67	1002.5	982.55	542.5	542.5
GW_REVAP	0.04	0.02	0.09	0.08	0.02	0.02	0.03	0.03

4.4 Trend Analysis in Sub-basin Scale

The MK test results at the sub-basin level provide the trends of change in GW and BW and associated significance levels as shown in Figures 4.6 and 4.7. Nearly two thirds of the sub-basins in ORB have experienced GW increase, and 49 sub-basins have very significant increasing trends (Fig.4.7). Approximately half sub-basins have experienced BW increase, and 13 sub-basins have very significant increasing trends (Fig.4.8). In the northwestern and middle northeastern region of ORB, most sub-basins show significant increasing trends in GW. The sub-basins in middle and very eastern ORB do not show any detectable GW change, whereas the southern sub-basins show decreasing GW trends over time. The spatial distribution of GW trend is more prominent than that of BW. Nevertheless, most significant increasing trends in BW are clustered in the northwestern, middle, and northeastern part of ORB. Decreasing trends of BW are widely distributed in the whole basin, and the proportion of sub-basins without clear trend in BW is slightly higher throughout ORB compared to the proportion in GW.

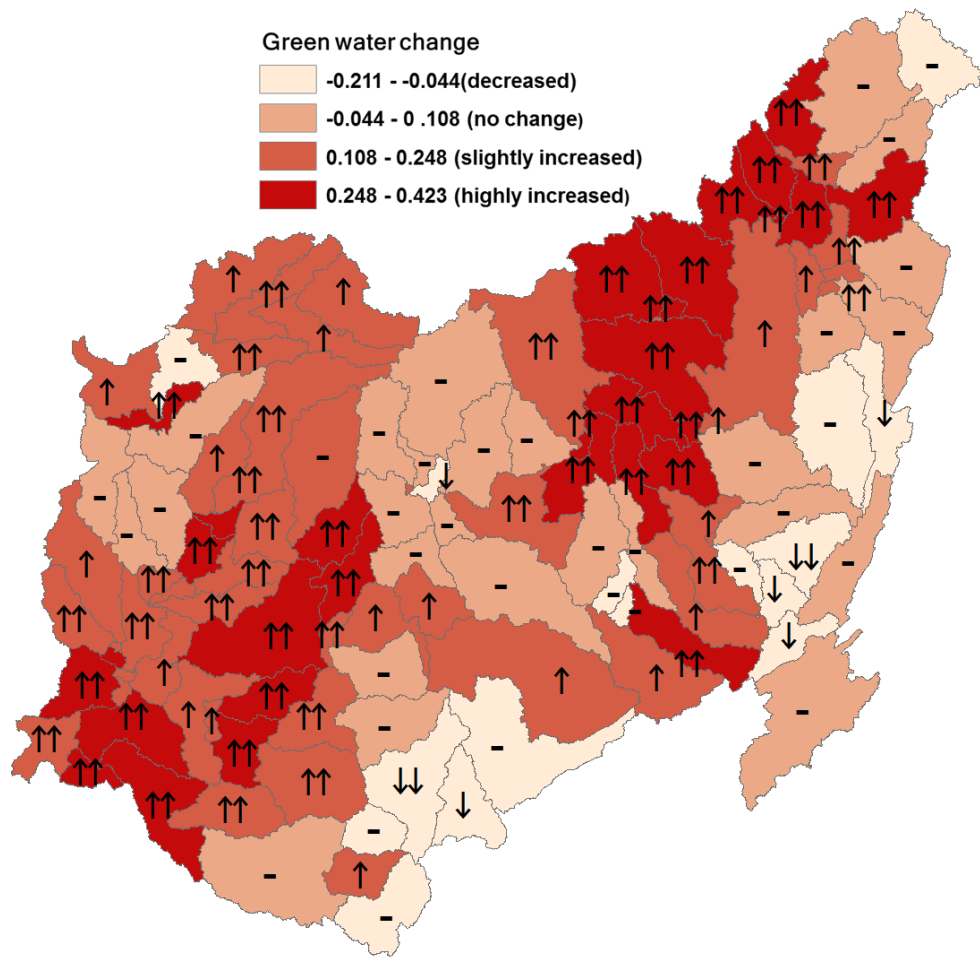


Figure 4.7 MK Test for GW in the Sub-basin Scale⁶

⁶ Colors represent decreasing or increasing trends, where darker color indicates higher tau (τ) value; arrows represent the significance level. "-": trend not significant, "↑": significant increase (p<0.1), "↑↑": very significant increase (p<0.01), "↓": significant decrease (p<0.1), and "↓↓": very significant decrease (p<0.01).

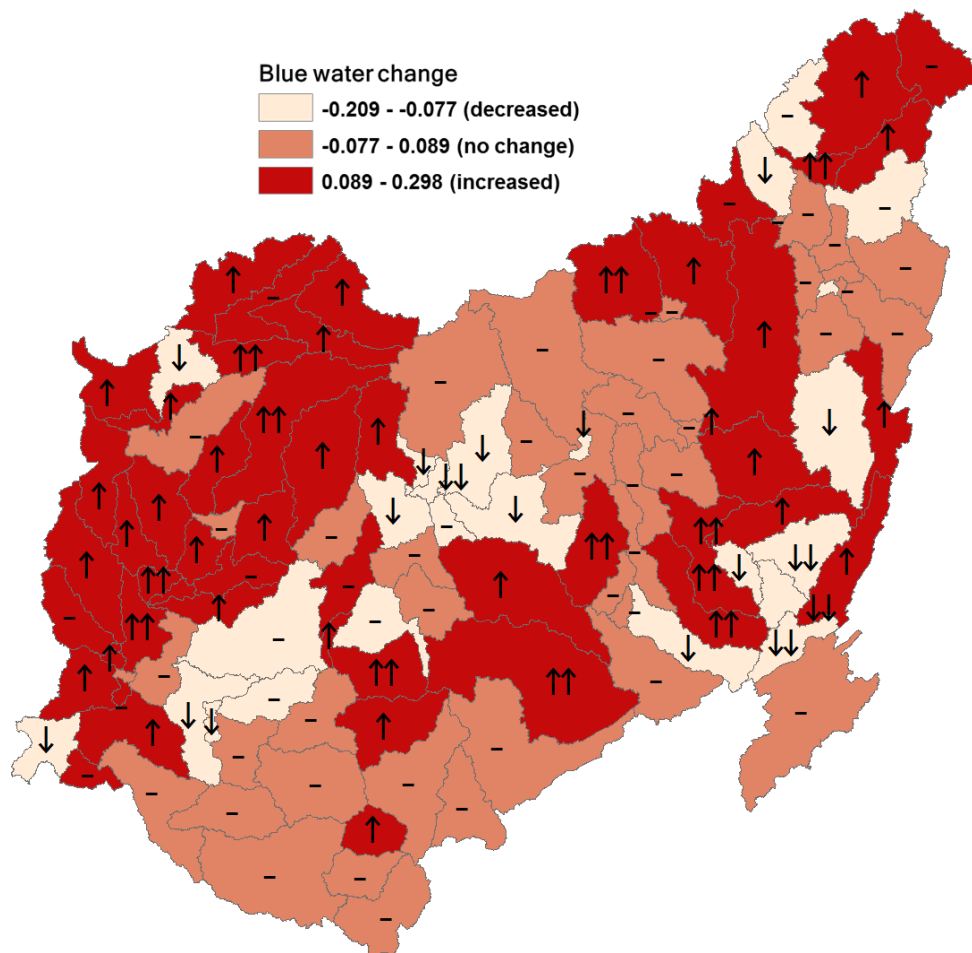


Figure 4.8 MK Test for BW in the Sub-basin Scale⁷

The spatial patterns of BW and GW in the sub-basin scale reveal that both BW and GW changes are caused by the combined effects of climate and land use. BW trends are dominantly affected more by precipitation change, whereas land use change has more impact on GW trends. For example, significant change of trends (either increasing or decreasing) in GW ($p < 0.01$) is found in the sub-basins with land use changes, such as in

⁷ Colors represent decreasing or increasing trends, where darker color indicates higher tau (τ) value; arrows represent the significance level. "-": trend not significant, "↑": significant increase ($p < 0.1$), "↑↑": very significant increase ($p < 0.01$), "↓": significant decrease ($p < 0.1$), and "↓↓": very significant decrease ($p < 0.01$).

the southwest and northeast. Specifically, among the 43 sub-basins with land use change, 35 show very significant increasing trends in GW (Fig. 4.6; Fig. 4.7).

For some of the sub-basins in the southern portion of both middle and upper regions, where no significant land use change has been detected, the decrease in precipitation is likely the main driver for the decreasing trend in GW (Fig. 4.6). Similarly, in most of the northeastern sub-basins where precipitation has increased noticeably but little land use change happens there, BW trends have also increased remarkably (Fig. 4.6; Fig. 4.8). However, some of the sub-basins in the northeast with increased precipitation and noticeable land use changes show a decrease or no trend in BW. In these areas, increased precipitation and land use change (agriculture to forest) may be counteracting with each other so no significant trend exists in BW.

In summary, BW increases in most sub-basins where precipitation has also increased; on the other hand, GW decreases in the sub-basins where land use change is not obvious but precipitation decreases. As a result, it could be inferred that in ORB precipitation change has a positive correlation with both BW and GW. That is, precipitation increase in ORB leads to the increase in both BW and GW, although the extent of impacts on GW is smaller. Similarly, land use change from agriculture to forest in the majority of sub-basins has caused an increase in GW, but a decrease in BW. These findings are further ascertained in terms of the relative effects of climate and land use change in the next section.

4.5 Trend analysis in Basin and Regional Scale

For the entire basin, the annual average values of both GW and BW have increased during the study period (Fig. 4.9 and Fig. 4.11; Table 4.6). According to the average TS slope, GW has increased by 27.3 km³ through the entire period, and the volumetric increase is 8% of the total GW volume in 1935. This trend is very significant according to the MK test ($p < 0.01$). The 95% confidence interval from TS test is also shown in Figure 4.11. Although BW has increased by 15 km³ according to the TS result, which accounts for 9% of the total BW values in 1935, the MK test suggests that this increasing trend is not significant ($p > 0.1$).

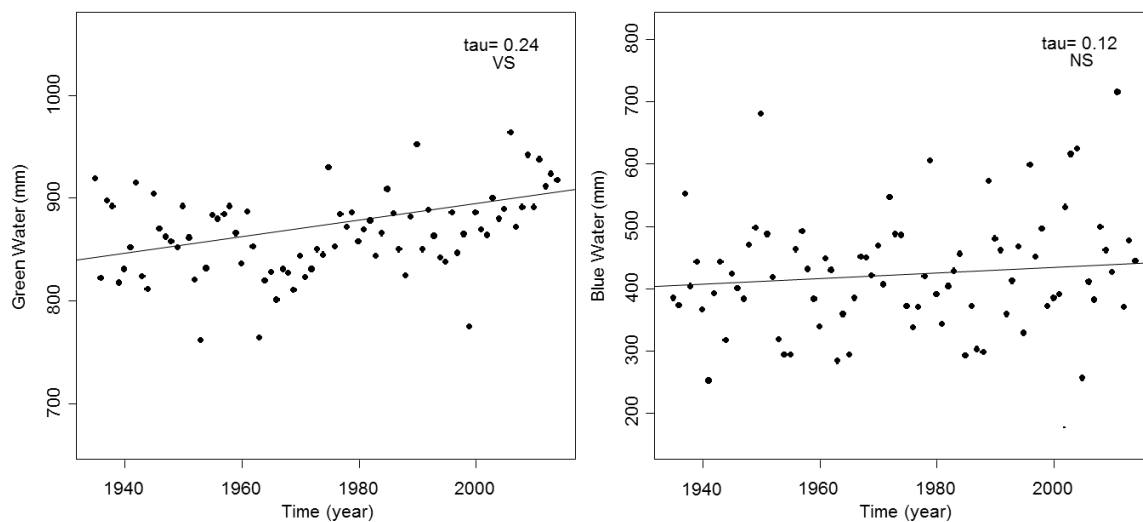


Figure 4.9 MK Test with TS Slope for BW and GW in the Basin Scale⁸

⁸ Tau is the Kendall rank correlation coefficient (τ). NS means not significant in MK test; S means significant at $p < 0.1$; VS means significant at $p < 0.01$.

Figure 4.10 and Table 4.6 present the trend analysis results for three regions separately. First, the middle region shows the least change in both BW and GW trends, which can be related to the invariable land use and climate in this region. Contrary to the other two regions, BW in the middle region is slightly decreasing as the precipitation over 78% of its area shows either decreasing or unchanged trends. The lower region shows the most significant increasing trends in both BW and GW in response to the pronounced change in both land use and climate: GW has increased by 12.78 km³ with a very significant MK trend ($p < 0.01$), and BW has increased by 11.22 km³ with a significant MK trend ($p < 0.1$). Similarly in the upper region, along with the prominent land use changes, GW has increased by 7.7 km³ with a significant MK trend ($p < 0.1$). The upper region also shows an insignificant increasing trend in BW in response to the relatively smaller changes in precipitation in this region compared to that in the lower region.

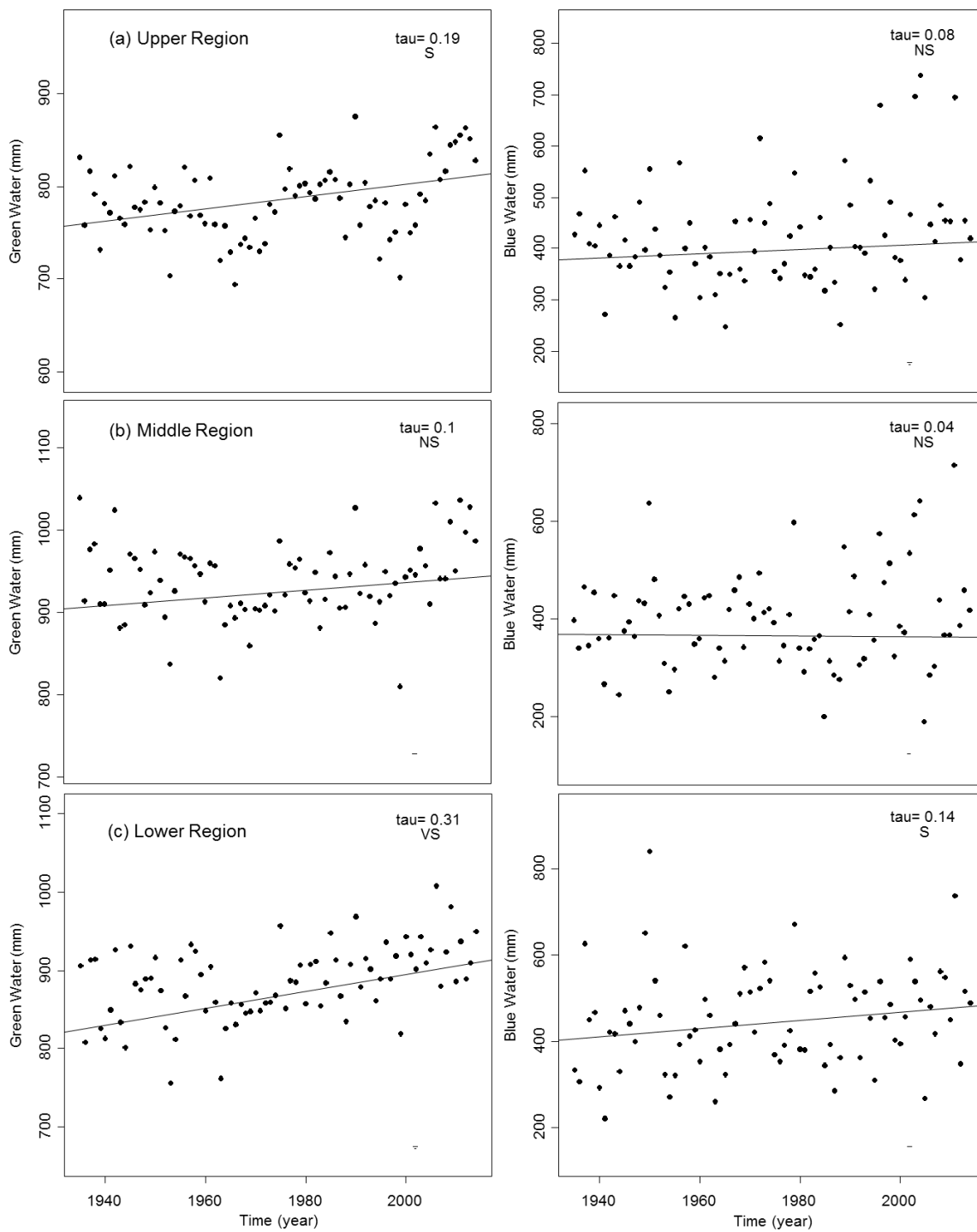


Figure 4.10 MK Test with TS Slope for BW and GW in the Regional Scale

Table 4.6 Volumetric Magnitudes of BW and GW Changes⁹

(km ³)	Entire Basin		Upper Region		Middle Region		Lower Region	
	GW	BW	GW	BW	GW	BW	GW	BW
Total Change	27.3*	15	7.7 ⁺	5	4.53	-0.64	12.78*	11.22 ⁺

Figure 4.11 shows the volumetric magnitudes of BW and GW change at the basin and regional levels based on the average TS slope with 95% confidence interval. Hollow points indicate the volumetric changes of BW and GW from average TS slope, which are the volumetric values used for further separation of climate and land use effects. The dark blue lines show 95% confidence intervals of total BW and GW change due to both climate and land use change, and the light blue lines show 95% confidence intervals of BW and GW change due solely to climate change. Except in the middle region, both BW and GW have increased in two different configurations. Excluding the insignificant change in the middle region, BW change due to combined effects is generally smaller than the change solely due to climate effects. The increase in GW due to climate change is relative small compared to the increase in BW, but the total increase of GW due to the combined effects is pretty large. This indicates that climate change has a more substantial impact on BW than GW, and land use change leads to a decrease in BW but an increase in GW.

⁹ "*": significant at p<0.01, "+": significant at p<0.1.

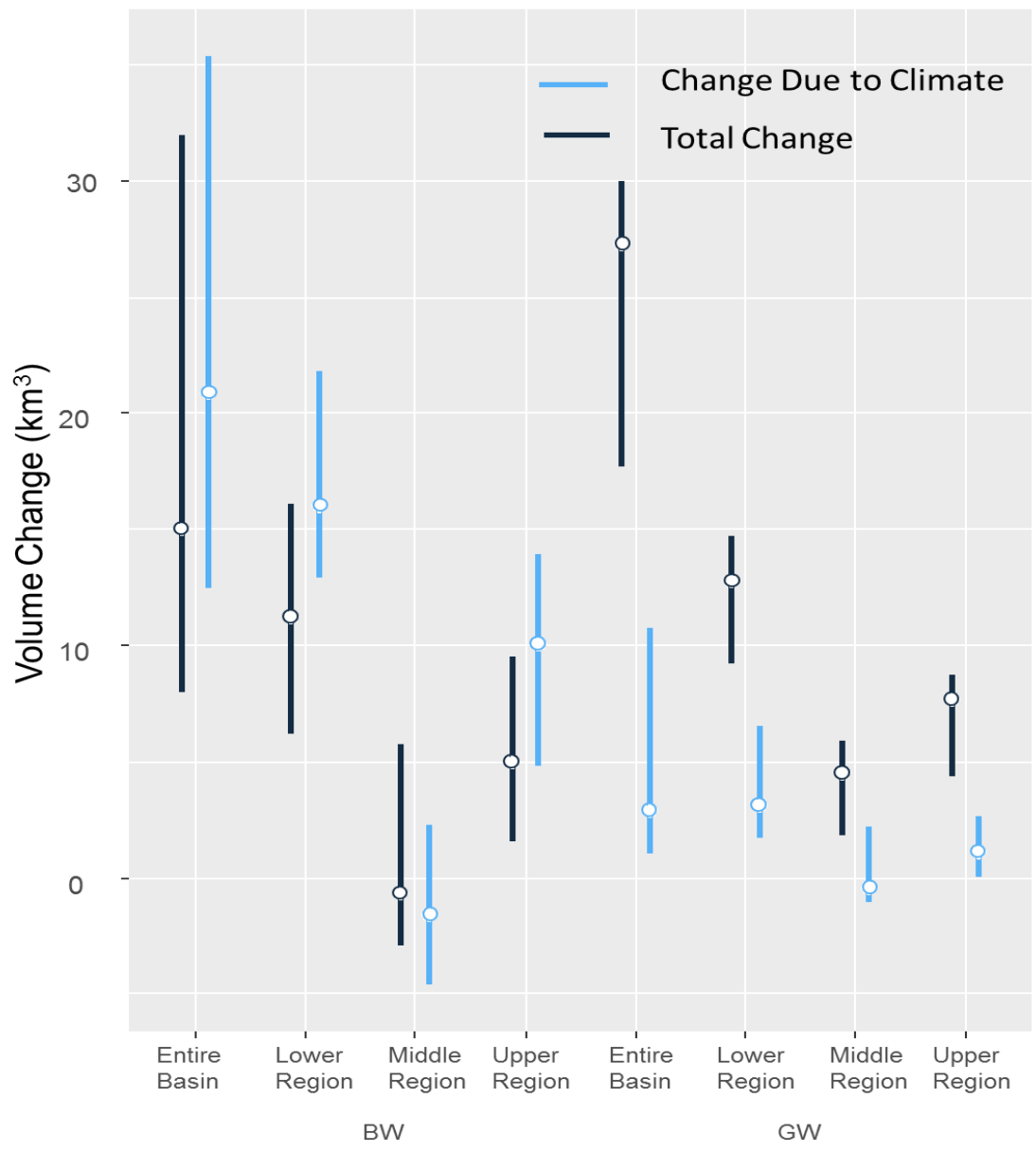


Figure 4.11 Volumetric Magnitudes of BW and GW with Confidence Interval

4.6 Relative Contributions of Climate and Land Use Change

The method to quantify the relative contributions of climate or land use effects on BW and GW are discussed in Section 3.6. The results in Table 4.7 show that the land use

change has caused 89% of the increase in annual GW values throughout the entire basin. At the regional scale, land use change alone has led to decreases in BW values by 34% and 23% in the upper and lower regions, respectively. However, due to the combined effect of precipitation increase and forest regrowth, the overall BW has increased slightly. The slight decrease in precipitation in the middle region has led to a decrease in BW and GW by 63% and 8%, respectively. The land use change in this region is responsible for most of the GW increase (92%). Nevertheless, the contributions of climate and land use change in the middle region are unclear because neither climate nor land use change is significant in this region.

Table 4.7 Relative Contributions to BW and GW¹⁰

	(km ³)	Total Change	Change by Climate	Climate Impacts	Land Use Impacts
Entire Basin	GW	27.3*	2.91	11%	89%
	BW	15.0	20.9 ⁺	78%	(-)22%
Upper Region	GW	7.7 ⁺	1.12	15%	85%
	BW	5.00	10.14	66%	(-)34%
Middle Region	GW	4.53	-0.43 ⁺	(-)8%	92%
	BW	-0.64	-1.60	(-) 63%	38%
Lower Region	GW	12.78*	3.11 ⁺	24%	76%
	BW	11.22 ⁺	16*	77%	(-)23%

Accordingly, the relative contributions of climate and land use change to BW and GW in Table 4.7 further support the major results derived from previous sections that climate change can affect both BW and GW. Climate change has a more pronounced effect on BW, whereas land use change in ORB has a stronger influence on the GW dynamics.

Table 4.6 shows the relative impacts of climate and land use change on the individual components of BW and GW, including total water yield, deep aquifer recharge, soil water content and ET over the entire ORB. Land use change is responsible for the increase in

¹⁰ "*": significant at p<0.01, "+": significant at p<0.1. Negative sign (-) means that resultant impact leads to a decrease.

ET and deep aquifer recharge by 99% and 55%, respectively, and it also leads to a moderate decrease in soil water content (31%) and a slight decrease in total water yield (15%). Climate change, or precipitation change in this study, is responsible for the substantial increase in soil water content (69%), total water yield (85%), and deep aquifer recharge (45%), but it has little influence on ET (1%).

Table 4.8 Relative Contributions to Each Water Component of BW and GW¹¹

(km ³)	Total Change	Change by Climate	Climate Impacts	Land Use Impacts
Total Water Yield	17.23	21.06 ⁺	85%	(-)15%
Deep Aquifer Recharge	0.87 ⁺	0.39 ⁺	45%	55%
Soil Water	4.22 ⁺	7.61*	69%	(-)31%
Actual Evapotranspiration	14.73 ⁺	-0.12	(-)1%	99%

¹¹ "*": significant at p<0.01, "+": significant at p<0.1. Negative sign (-) means that resultant impact leads to a decrease.

CHAPTER 5. DISCUSSION

The results from this study as presented in Chapter 4 show that the combined effects of climate and land use change has led to increasing BW and GW trends in ORB from 1935 to 2014. Climate change has a more substantial effect on BW, but a relatively small impact on GW. Land use change from agriculture to forest increases GW remarkably, but decreases BW. In this chapter, the results from this study are further discussed within the context of previous studies. In addition, the uncertainties and limitations of this study are also included. In Section 5.7, a general future forecast of BW and GW is presented based on previous studies on future climate and land use change in ORB.

5.1 Climate Impacts on BW

In this study, the effect of climate on BW or GW primarily refers to the change in precipitation because annual average temperature change is not significant in ORB. If the effect of land use is excluded, precipitation increase will raise the soil moisture store level and consequently increase the runoff volume. With more water available to vadose zone, groundwater flow and thereby deep aquifer recharge will increase. For the entire basin, an 8% increase of precipitation leads to an 11% increase in BW. This result is generally consistent to the result of previous study on 1337 basins throughout the USA

that a 1% change in precipitation results in a 1.5-2.5% change in runoff (Sankarasubramanian & Vogel, 2003). Although the effects of temperature changes are not considered in this study, previous studies suggest both temperature and precipitation are critical to both BW and GW (Abbaspour et al., 2009; Fu et al., 2007; Jha et al., 2004; Legesse et al., 2003; van Roosmalen et al., 2009). According to Fu et al. (2007), an increase in streamflow due to precipitation increase is weakened by average temperature increase. In addition, despite insignificant change in average temperature, the rising minimum temperature may still impact hydrologic responses in the northeastern part, more specifically in terms of volume and timing of snow melt, thereby increasing the surface runoff to some extent.

5.2 Climate Impacts on GW

Despite the overall GW increase in ORB, climate has opposing impact on soil water content and ET. Specifically, climate change increases soil water content, but has little or negative effect on ET. The influence of climate on soil water content is consistent with findings from previous studies that report increasing precipitation increases the water content in unsaturated soils. However, unlike this study, some previous studies report a positive correlation between precipitation and ET (Claessens et al., 2006; Gosain et al., 2006; Li et al., 2009).

As is known, ET is dominated by potential evapotranspiration (PET) and precipitation, and the amount of ET is strictly limited by the minimal value of the two factors. On possible reason might be that most of the previous BW and GW studies focus on arid or

semi-arid areas (Abbaspour et al., 2009; Faramarzi et al., 2013; Li et al., 2009), where ET is largely limited by the amount of available water. The amount of ET in those regions is very sensitive to precipitation increase. On the contrary, the amount of annual PET is close to or even smaller than annual precipitation in ORB, so ET is governed by PET even though precipitation has increased. The weak correlation between precipitation increase and ET increase has also been found in Illinois River Basin (Niemann & Eltahir, 2005), where the climate is similar to that in ORB.

5.3 Land Use Impact on BW

The characteristic land use change in ORB during the study period is the conversion from croplands to forests, and it accounts for the slight decrease in BW, especially the total water yield. Compared with agricultural vegetation, trees generally have deeper roots and hence have higher plant-available water capacity, which determines the ability of plants to draw water from soils (Zhang et al., 2001). As a result, these second-grown trees extract more rainfall than crops do, decreasing surface runoff and ground water recharge in the wet periods, and decreasing the content of soil moisture in the dry seasons.

Although the results show an increase in deep aquifer recharge, the reported change is based on the simulated output for the specific study period. In reality, change in deep aquifer storage is a much slower process. Besides, the model result does not consider the detail input of aquifers' geologic characteristics. Therefore, the change of deep aquifer recharge might be overestimated in this study.

5.4 Land use impact on GW

A great portion of GW increase comes from land use change. As mentioned in Section 5.3, forests can extract more rain water for transpiration than crops, which thereby increases GW flow (ET) and decrease GW storage (soil water content). Although land use change is largely responsible for GW change and partially for BW change in this study, the effects of land use change on BW and GW at a basin level might be underestimated due to the compensating effects in a complex catchment (Fohrer et al., 2001). The complex interactions between different vegetation types weaken land use effects in a large and complex catchment compared to the effects in a small and uniform vegetated catchment. Fohrer et al. (2002) document that the land use type from forests to crops (barley in his study) reduces the ET to 69% with the exclusion of the compensating effects, but this reduction is offset in a catchment scale. ET increase due to land use change is about 5% of the overall ET in the basin scale, and the increase may be larger in the sub-basin scale.

5.5 Uncertainty Analysis

Three kinds of uncertainties will be discussed in this section: the uncertainty from data input, from model concept and from statistical analysis. In this study, 112 weather stations are selected in a manner such that each of the 125 sub-basins has one station within or at the proximity of its respective boundary, maintaining a uniform spatial distribution of stations over the entire ORB. Nevertheless, the resultant precipitation fields can be very uncertain because on average every weather station covers 4383 km² of

the study area. In addition, input topography, soil and land use data used in this study have 90 m horizontal resolution, and such coarse resolution also adds uncertainty to the overall model results.

Model uncertainty usually comes from model structure and parameters. Model structure uncertainty can come from some unknown activities in a watershed which are not considered in the model, or some simplifications of the processes. Although the calibration results from this study are acceptable based on commonly used performance measures such as KGE and NS, use of a limited number of stream locations for calibration in such a large basin can introduce equifinality problem. Similarly, only streamflow is calibrated and validated in this study, which leads to uncertainties in the output of ground water, ET, deep aquifer recharge, and total water yield. Finally, in order to quantify contributions of climate change and land use changes, this study assumes that constant land use does not influence the sensitivity and uncertainties of SWAT parameters. However, as SWAT is not a truly physics based model, keeping land use constant may lead to a change in SWAT parameters.

It should be noted that although the relative contributions of climate and land use effects have been quantified in terms of percentage, there is considerable uncertainty in the values. Despite the confidence intervals shown in Figure 4.10, the upper and lower bounds of volumetric changes are not considered when the relative contributions are calculated. Furthermore, since the confidence level of total BW change due to climate and land use effects in the basin level overlaps with the interval due solely to climate

effect, the statistical difference of BW change between the two configurations is not distinguished. The impact of land use change on BW might be overestimated. Therefore, the relative contributions of climate and land use effects on BW in the basin scale should be considered conservatively.

5.6 Limitations

Many of the past studies on large scale BW and GW dynamics assume a constant land use over a long time period of simulation (Abbaspour et al., 2009; Chen et al., 2014; Zang & Liu, 2013). With the use of time-varying land use in SWAT simulation, the current study offsets the aforementioned limitation and hence, the modeled outputs are expected to be more representative of the actual hydrologic responses. However, certain limitations still exist in this study.

First, reservoir management is not considered due to the lack of operation data over the entire 80 years. In addition, the existence of dams/locks restricts the usage of many available USGS streamflow gauge stations along the main channel of the Ohio River in model calibration. Although the calibration results are quite satisfactory, a limited number of stream locations for calibration in such a large basin introduces the problem of equifinality. Furthermore, only streamflow is calibrated and validated due to the lack of data in soil water content, ground water, and ET, which increases the uncertainties associated with BW and GW simulated outputs.

Second, the accuracy of SWAT model is affected by the coarse resolution of data and model simplification. A 90m horizontal resolution for raster grids and a 2,500 km² critical source area threshold is reasonable for such a large basin, but still such a coarse resolution is not sufficient for further detailed analysis. As this study uses sub-basin rather than HRU as the smallest unit of simulation, many of the complex interactions among hydrologic fluxes is averaged out, which might lead to imprecise assessment of climate, land use, BW and GW change. Although HRU-scale simulation could represent the spatial heterogeneity more accurately, it would cost great computational resources and time for such a large scale model.

Third, using the same spatial coverage of artificial subsurface (tile) drainage over the entire period of simulation since 1935 does not represent the gradual change in tile drainage over time, but the effect of tile drainage over the calculated volumetric change in long-term BW and GW may be minimal. This study doesn't consider agricultural operations such as plant growth and tillage, which could influence surface runoff, infiltration, and soil water content by changing soil porosity and surface roughness (Moussa et al., 2002).

Finally, despite daily simulation, this study presents results based only on average annual values. However, more detailed characterization with seasonal change pattern and trend analysis would provide a thorough understanding of the overall dynamics of BW and GW in ORB.

5.7 Future Forecast

Future change of BW and GW are expected to be different from historical trends because of different future climate and land use change. The temperature in ORB is expected to rise due to global warming (Stocker et al., 2013). Although the overall future precipitation trend remains unclear, increasing precipitation extremes are bound to influence hydrologic process in ORB. It is estimated that in 2050, urban areas for ORB will reach 11.83% while the respective portion of agriculture and forest will decrease to 35.8% and 47.6% (Tayyebi et al., 2015). The combined effects of future climate and land use changes probably will lead to a further increase in BW but a decrease in GW. However, further studies are necessary in order to quantify the future patterns of BW and GW in ORB.

CHAPTER 6. SUMMARY AND CONCLUSION

This study performs a spatio-temporal characterization of climate and land use change impacts on the Blue Water (BW) and Green Water (GW) availability in the Ohio River Basin (ORB). Total nine SWAT models are created under the 'variable climate-variable land use' and 'variable climate-steady land use' configurations in order to quantify the combined as well as the relative impacts of climate and land use change in altering the dynamics of BW and GW over a 80 year period (1935-2014). The following conclusions can be drawn from this study.

First, precipitation increase and land use change from agriculture to forest are detected as the dominant indicators of climate and land use change in ORB, respectively. While land use and climate changes are evident in the upper (upstream) and lower (downstream) regions during the 80 years of study, the middle region is least impacted in terms of both climate and land use.

Second, under the combined influence of climate and land use (variable climate-variable land use) model configuration, the annual values of BW and GW over the entire basin have increased by 15 km^3 and 27.3 km^3 from 1935 to 2014, respectively. The lower region exhibits maximum changes, where the increasing trends for both BW and GW are

found statistically significant in response to the pronounced change both in land use and climate. Similarly, in conjunction with the prominent land use changes in the upper region, GW has increased significantly. BW is found to have increased there as well, but the trend of change is not significant, which corresponds to the relatively smaller changes in precipitation amount in the upper region compared to that in the lower region.

Similarly, least changes in both BW and GW are observed in the middle region due to the unclear climate and land use change there.

Finally, by separating the individual contributions of climate and land use change in the 'variable climate-steady land use' model configuration, a causal relationship is deduced showing that land use change in ORB generally has a stronger impact on the dynamics of GW, while climate change affects both BW and GW but it is more sensitive to BW.

Overall, this study identifies the areas or regions within ORB that have experienced major changes in the spatio-temporal dynamics of BW and GW as a consequence of prevailing climate and land use changes. The sub-basin scale spatial variability and sensitivity analysis presented here will help to initiate management strategies suitable for specific regions. Relative impacts of climate and land use change in changing the dynamics of BW and GW in this study will allow policymakers to take the mitigating measures in a more efficient and targeted way depending on whether climate change or land use change is the governing factor for a region of interest. Although the paper reveals the spatio-temporal pattern of changes in BW and GW over a considerable time length of past records (1935-2014), evaluation of their plausible future variability using

different climate model and land use projections deserves high priority, considering the basin's overall socio-economic importance. Until then, the findings from this study can be adopted as the baseline reference for future water security research and planning.

LIST OF REFERENCES

LIST OF REFERENCES

- Abbaspour, K. (2013). SWAT-CUP 2012: SWAT calibration and uncertainty programs- A user manual. *Eawag Swiss Federal Institute of Aquatic Science and Technology*.
- Abbaspour, K., Johnson, C., & Van Genuchten, M. T. (2004). Estimating uncertain flow and transport parameters using a sequential uncertainty fitting procedure. *Vadose Zone Journal*, 3(4), 1340-1352.
- Abbaspour, K., Rouholahnejad, E., Vaghefi, S., Srinivasan, R., Yang, H., & Kløve, B. (2015). A continental-scale hydrology and water quality model for Europe: Calibration and uncertainty of a high-resolution large-scale SWAT model. *Journal of Hydrology*, 524, 733-752.
- Abbaspour, K. C., Faramarzi, M., Ghasemi, S. S., & Yang, H. (2009). Assessing the impact of climate change on water resources in Iran. *Water Resources Research*, 45(10).
- Allen, R. G., Pereira, L. S., Raes, D., & Smith, M. (1998). Crop evapotranspiration- Guidelines for computing crop water requirements-FAO Irrigation and drainage paper 56. *FAO, Rome*, 300(9), D05109.
- Asselen, S., & Verburg, P. H. (2013). Land cover change or land - use intensification: simulating land system change with a global - scale land change model. *Global change biology*, 19(12), 3648-3667.
- Boles, C. M. W. (2013). Swat model simulation of bioenergy crop impacts in a tile-drained watershed.
- Chen, C., Hagemann, S., & Liu, J. (2014). Assessment of impact of climate change on the blue and green water resources in large river basins in China. *Environmental Earth Sciences*, 1-14.
- Claessens, L., Hopkinson, C., Rastetter, E., & Vallino, J. (2006). Effect of historical changes in land use and climate on the water budget of an urbanizing watershed. *Water Resources Research*, 42(3).

- Du, B., Arnold, J., Saleh, A., & Jaynes, D. (2005). Development and application of SWAT to landscapes with tiles and potholes. *Transactions of the ASAE*, 48(3), 1121-1133.
- Eshleman, K. N. (2004). Hydrological Consequences of Land Use Change: A Review of the State - of - Science. *Ecosystems and Land Use Change*, 13-29.
- Falkenmark, M. (1995). *Coping with water scarcity under rapid population growth*. Paper presented at the Conference of SADC ministers, Pretoria.
- Falkenmark, M., & Rockström, J. (2006). The new blue and green water paradigm: Breaking new ground for water resources planning and management. *Journal of water resources planning and management*.
- Faramarzi, M., Abbaspour, K. C., Schulin, R., & Yang, H. (2009). Modelling blue and green water resources availability in Iran. *Hydrological Processes*, 23(3), 486-501.
- Faramarzi, M., Abbaspour, K. C., Vaghefi, S. A., Farzaneh, M. R., Zehnder, A. J., Srinivasan, R., & Yang, H. (2013). Modeling impacts of climate change on freshwater availability in Africa. *Journal of Hydrology*, 480, 85-101.
- Fohrer, N., Haverkamp, S., Eckhardt, K., & Frede, H.-G. (2001). Hydrologic response to land use changes on the catchment scale. *Physics and Chemistry of the Earth, Part B: Hydrology, Oceans and Atmosphere*, 26(7), 577-582.
- Fohrer, N., Möller, D., & Steiner, N. (2002). An interdisciplinary modelling approach to evaluate the effects of land use change. *Physics and Chemistry of the Earth, Parts A/B/C*, 27(9), 655-662.
- Fu, G., Charles, S. P., & Chiew, F. H. (2007). A two - parameter climate elasticity of streamflow index to assess climate change effects on annual streamflow. *Water Resources Research*, 43(11).
- Glavan, M., Pintar, M., & Volk, M. (2013). Land use change in a 200 - year period and its effect on blue and green water flow in two Slovenian Mediterranean catchments—lessons for the future. *Hydrological Processes*, 27(26), 3964-3980.
- Goldewijk, K. K. (2001). Estimating global land use change over the past 300 years: the HYDE database. *Global Biogeochemical Cycles*, 15(2), 417-433.
- Gosain, A., Rao, S., & Basuray, D. (2006). Climate change impact assessment on hydrology of Indian river basins. *Current science*, 90(3), 346-353.

- Green, C., Tomer, M., Di Luzio, M., & Arnold, J. (2006). Hydrologic evaluation of the soil and water assessment tool for a large tile-drained watershed in Iowa. *Transactions of the ASAE*, 49(2), 413-422.
- Gupta, H. V., Kling, H., Yilmaz, K. K., & Martinez, G. F. (2009). Decomposition of the mean squared error and NSE performance criteria: Implications for improving hydrological modelling. *Journal of Hydrology*, 377(1), 80-91.
- Gupta, S. C., Kessler, A. C., Brown, M. K., & Zvomuya, F. (2015). Climate and agricultural land use change impacts on streamflow in the upper midwestern United States. *Water Resources Research*, 51(7), 5301-5317.
- Hamed, K. (2009). Exact distribution of the Mann–Kendall trend test statistic for persistent data. *Journal of Hydrology*, 365(1), 86-94.
- Hamed, K. H. (2008). Trend detection in hydrologic data: the Mann–Kendall trend test under the scaling hypothesis. *Journal of Hydrology*, 349(3), 350-363.
- Hamed, K. H., & Rao, A. R. (1998). A modified Mann-Kendall trend test for autocorrelated data. *Journal of Hydrology*, 204(1), 182-196.
- Jaynes, D., & James, D. (2007). The extent of farm drainage in the United States. *US Department of Agriculture*.
- Jewitt, G., Garratt, J., Calder, I., & Fuller, L. (2004). Water resources planning and modelling tools for the assessment of land use change in the Luvuvhu Catchment, South Africa. *Physics and Chemistry of the Earth, Parts A/B/C*, 29(15), 1233-1241.
- Jha, M., Pan, Z., Takle, E. S., & Gu, R. (2004). Impacts of climate change on streamflow in the Upper Mississippi River Basin: A regional climate model perspective. *Journal of Geophysical Research: Atmospheres (1984–2012)*, 109(D9).
- Kendall, M. G. (1948). Rank correlation methods.
- Kendall, M. G., & Gibbons, J. D. (1990). Rank correlation methods.
- Kling, H., Fuchs, M., & Paulin, M. (2012). Runoff conditions in the upper Danube basin under an ensemble of climate change scenarios. *Journal of Hydrology*, 424, 264-277.

- Kumar, S., Merwade, V., Kam, J., & Thurner, K. (2009). Streamflow trends in Indiana: effects of long term persistence, precipitation and subsurface drains. *Journal of Hydrology*, 374(1), 171-183.
- Larose, M., Heathman, G., Norton, L., & Engel, B. (2007). Hydrologic and atrazine simulation of the Cedar Creek watershed using the SWAT model. *Journal of environmental quality*, 36(2), 521-531.
- Legesse, D., Vallet-Coulomb, C., & Gasse, F. (2003). Hydrological response of a catchment to climate and land use changes in Tropical Africa: case study South Central Ethiopia. *Journal of Hydrology*, 275(1), 67-85.
- Lettenmaier, D. P., Wood, E. F., & Wallis, J. R. (1994). Hydro-climatological trends in the continental United States, 1948-88. *Journal of Climate*, 7(4), 586-607.
- Li, L., Zhang, L., Xia, J., Gippel, C. J., Wang, R., & Zeng, S. (2015). Implications of modelled climate and land cover changes on runoff in the middle route of the south to north water transfer project in China. *Water Resources Management*, 29(8), 2563-2579.
- Li, Z., Liu, W.-z., Zhang, X.-c., & Zheng, F.-l. (2009). Impacts of land use change and climate variability on hydrology in an agricultural catchment on the Loess Plateau of China. *Journal of Hydrology*, 377(1), 35-42.
- Liu, X.-f., Ren, L., Yuan, F., Singh, V., Fang, X., Yu, Z., & Zhang, W. (2009). Quantifying the effect of land use and land cover changes on green water and blue water in northern part of China. *Hydrology and Earth System Sciences*, 13(6), 735-747.
- Mann, H. B. (1945). Nonparametric tests against trend. *Econometrica: Journal of the Econometric Society*, 245-259.
- Meehl, G. A., Stocker, T. F., Collins, W. D., Friedlingstein, P., Gaye, A. T., Gregory, J. M., . . . Noda, A. (2007). Global climate projections. *Climate change*, 283.
- Mishra, V., Cherkauer, K. A., Niyogi, D., Lei, M., Pijanowski, B. C., Ray, D. K., . . . Yang, G. (2010). A regional scale assessment of land use/land cover and climatic changes on water and energy cycle in the upper Midwest United States. *International Journal of Climatology*, 30(13), 2025-2044.
- Moussa, R., Voltz, M., & Andrieux, P. (2002). Effects of the spatial organization of agricultural management on the hydrological behaviour of a farmed catchment during flood events. *Hydrological Processes*, 16(2), 393-412.

- Neitsch, S. L., Arnold, J. G., Kiniry, J. R., & Williams, J. R. (2011). Soil and water assessment tool theoretical documentation version 2009: Texas Water Resources Institute.
- Niemann, J. D., & Eltahir, E. A. (2005). Sensitivity of regional hydrology to climate changes, with application to the Illinois River basin. *Water Resources Research*, 41(7).
- O'Donnell, G. M., Czajkowski, K. P., Dubayah, R. O., & Lettenmaier, D. P. (2000). Macroscale hydrological modeling using remotely sensed inputs: Application to the Ohio River basin. *Journal of Geophysical Research: Atmospheres (1984–2012)*, 105(D10), 12499-12516.
- Rahman, M. M., Lin, Z., Jia, X., Steele, D. D., & DeSutter, T. M. (2014). Impact of subsurface drainage on streamflows in the Red River of the North basin. *Journal of Hydrology*, 511, 474-483.
- Rajib, M. A., & Merwade, V. (2015). Improving soil moisture accounting and streamflow prediction in SWAT by incorporating a modified time - dependent Curve Number method. *Hydrological Processes*.
- Rockström, J., Falkenmark, M., Karlberg, L., Hoff, H., Rost, S., & Gerten, D. (2009). Future water availability for global food production: the potential of green water for increasing resilience to global change. *Water Resources Research*, 45(7).
- Sankarasubramanian, A., & Vogel, R. M. (2003). Hydroclimatology of the continental United States. *Geophysical Research Letters*, 30(7).
- Schnitkey, G. (2013). The New Era of Crop Prices-A Five-Year Review." farmdoc daily (3): 38. *Department of Agricultural and Consumer Economics, University of Illinois at Urbana-Champaign*.
- Schuol, J., Abbaspour, K. C., Yang, H., Srinivasan, R., & Zehnder, A. J. (2008). Modeling blue and green water availability in Africa. *Water Resources Research*, 44(7).
- Sen, P. K. (1968). Estimates of the regression coefficient based on Kendall's tau. *Journal of the American Statistical Association*, 63(324), 1379-1389.
- Singh, J., Knapp, H. V., Arnold, J., & Demissie, M. (2005). Hydrological modeling of the iroquois river watershed using HSPF and SWAT1: Wiley Online Library.

- Stocker, T., Qin, D., Plattner, G.-K., Tignor, M., Allen, S. K., Boschung, J., . . . Midgley, P. M. (2014). *Climate change 2013: The physical science basis*: Cambridge University Press Cambridge, UK, and New York.
- Stocker, T., Qin, D., Plattner, G., Tignor, M., Allen, S., Boschung, J., . . . Midgley, B. (2013). IPCC, 2013: climate change 2013: the physical science basis. Contribution of working group I to the fifth assessment report of the intergovernmental panel on climate change.
- Tayyebi, A., Pijanowski, B. C., & Pekin, B. K. (2015). Land use legacies of the Ohio River Basin: Using a spatially explicit land use change model to assess past and future impacts on aquatic resources. *Applied Geography*, *57*, 100-111.
- van Roosmalen, L., Sonnenborg, T. O., & Jensen, K. H. (2009). Impact of climate and land use change on the hydrology of a large - scale agricultural catchment. *Water Resources Research*, *45*(7).
- Von Storch, H. (1999). *Misuses of statistical analysis in climate research*: Springer.
- White, D., Johnston, K., & Miller, M. (2005). Ohio river basin. *Rivers of North America*, 375-424.
- Winchell, M., Srinivasan, R., Di Luzio, M., & Arnold, J. (2010). ARCSWAT interface for Soil and Water Assessment Tool SWAT 2009. *User's Guide Texas AgriLife Research and USDA Agricultural Research Service, Temple, Texas-USA*.
- Xu, J. (2013). Effects of climate and land-use change on green-water variations in the Middle Yellow River, China. *Hydrological Sciences Journal*, *58*(1), 106-117.
- Yue, S., Pilon, P., Phinney, B., & Cavadias, G. (2002). The influence of autocorrelation on the ability to detect trend in hydrological series. *Hydrological Processes*, *16*(9), 1807-1829.
- Zang, C., & Liu, J. (2013). Trend analysis for the flows of green and blue water in the Heihe River basin, northwestern China. *Journal of Hydrology*, *502*, 27-36.
- Zang, C., Liu, J., Velde, M., & Kraxner, F. (2012). Assessment of spatial and temporal patterns of green and blue water flows under natural conditions in inland river basins in Northwest China. *Hydrology and Earth System Sciences*, *16*(8), 2859-2870.

- Zhang, L., Dawes, W., & Walker, G. (2001). Response of mean annual evapotranspiration to vegetation changes at catchment scale. *Water Resources Research*, 37(3), 701-708.
- Zhang, W., Zha, X., Li, J., Liang, W., Ma, Y., Fan, D., & Li, S. (2014). Spatiotemporal Change of Blue Water and Green Water Resources in the Headwater of Yellow River Basin, China. *Water Resources Management*, 28(13), 4715-4732.
- Zucker, L. A., & Brown, L. C. (1998). *Agricultural drainage: Water quality impacts and subsurface drainage studies in the Midwest* (Vol. 871): Ohio State University Extension.
- Zuo, D., Xu, Z., Peng, D., Song, J., Cheng, L., Wei, S., . . . Yang, H. (2015). Simulating spatiotemporal variability of blue and green water resources availability with uncertainty analysis. *Hydrological Processes*, 29(8), 1942-1955.